FACULTY OF BIOSCIENCE ENGINEERING

HYPERDIMENSIONAL COMPUTING FOR PROTEIN LANGUAGE MODELING

word count: 15663

Michael Fatjanov
Student ID: 01917077

Promotors: Prof. dr. Bernard De Baets & dr. ir. Michiel Stock
Supervisor: ir. Dimitri Boeckaerts

Dissertation submitted to Ghent University in partial fulfilment of the requirements for the degree of master in Bioinformatics (Systems Biology track).
Academic year: 2022-2023

GHENT UNIVERSITY

De auteur en promotor geven de toelating deze scriptie voor consultatie beschikbaar te stellen en delen ervan te kopiëren voor persoonlijk gebruik. Elk ander gebruik valt onder de beperkingen van het auteursrecht, in het bijzonder met betrekking tot de verplichting uitdrukkelijk de bron te vermelden bij het aanhalen van resultaten uit deze scriptie.

The author and promoter give the permission to use this thesis for consultation and to copy parts of it for personal use. Every other use is subject to the copyright laws, more specifically the source must be extensively specified when using results from this thesis.

Gent, 14-06-2023

The promotor,	The author,
Prof. dr. Bernard De Baets	Michael Fatjanov

ACKNOWLEDGEMENTS

Thank you, all of you!

CONTENTS

ABSTRACT

This dissertation explores the implementation and application of hyperdimensional computing for protein sequence analysis. We discussed the advancements of state-of-the-art protein language models in protein structure and function predictions while raising the need for more computationally and data-efficient methods. As hyperdimensional computing was proposed as a promising avenue, its underlying principles and mathematical operations were illustrated to demonstrate the potential of hyperdimensional computing in bioinformatics research.

We researched and developed several methods to encode amino acids into hyperdimensional vectors. Of these, projecting embeddings containing biological information into hyperdimensional space has proven itself to be useful in subsequent analyses and prediction tasks. Utilizing the PhaLP database [1], a continuously updated database of phage lytic proteins, we applied these amino acid encoding methods to develop techniques for protein sequence encodings. We demonstrate the capability of these methods to capture essential protein sequence information in hyperdimensional vectors, proving their usefulness in prediction tasks. In our classification tasks, we show that hyperdimensional computing-based learning methods displayed competitive performance when compared to established machine learning methods such as random forest and XGBoost. In addition, we examined perceptron-based models for context-aware protein residue learning, utilizing neighborhood-encoded hyperdimensional vectors. Although this did not outperform current state-of-the-art models, it contributed valuable insights into the challenges faced when implementing efficient models for such tasks within the hyperdimensional computing framework.

Finally, we acknowledge the need for continued research in refining our encoding algorithms, exploring alternative model architectures, and extending the scope of tasks and datasets. Despite mixed results, our findings lay a solid foundation for further investigation into hyperdimensional computing's potential in protein sequence research and bioinformatics.

1. INTRODUCTION

1.1 A historical perspective on bioinformatics

Many decades ago, around the 1950s, we did not know much about the molecules that carry our genetic information and how this would be translated into higher levels of biology. All that was known about deoxyribonucleic acid (DNA) was that it carries nucleotides in equimolar proportions so that there is as much guanine as cytodine and as much adenine as thymine. A major breakthrough came with J. Watson, F. Crick and R. Franklin's discovery of the structure of DNA in 1953 [2] [3]. Despite that, it took several more decades before the genetic code was deciphered and how this information is further processed. Researchers came to know that DNA is essentially built up of a linear sequence of the four aforementioned nucleic acids. This sequence encodes information that undergoes transcription into ribonucleic acid (RNA) which in turn gets translated into proteins. The encoding of proteins is done in groups of three nucleic acids at a time, known as codons. This was later summarized as the *central dogma of molecular biology*, also by Crick in 1958 [4]. This was hugely important for later research since it gives us more insight into how the genetic code is translated and transferred.

In the same decade, major leaps were made in the research of protein structure and sequences. The first three-dimensional protein structures were determined via X-ray crystallography [16], which is still to this day the preferred method. On top of that, the arrangement of the primary structure of a protein has been resolved after the first sequencing of a polypeptide. Sanger determined by sequencing [5] insulin in 1953 that a protein is built up of a sequence of amino acids, all connected by a peptide bond to form a polypeptide. This finding established the idea that proteins are biological macromolecules that carry lots of information [17], starting a boom of research on more efficient methods for obtaining protein sequences. The most popular method of that time was the Edman degradation method [18]. A major issue with this method was that only a theoretical maximum of 50

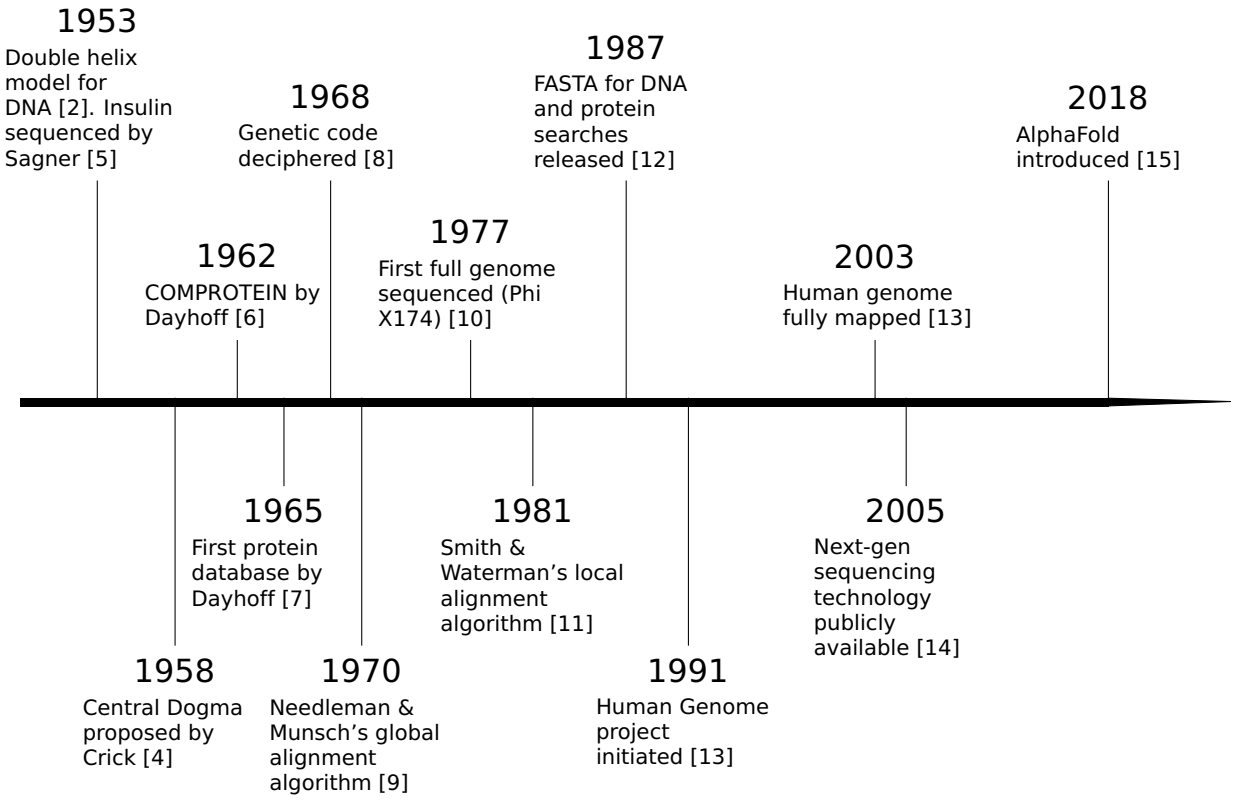

Figure 1.1: Timeline of important developments in bioinformatics.

to 60 sequential amino acids could be sequenced. Larger proteins had to be cleaved into fragments that were small enough to be sequenced. Tracing back the input sequence from this data was a cumbersome process and thus published Dayhoff the first computational program applied to biological data, COMPROTEIN [6] in 1962. This program was essentially a *de novo* sequence assembler for Edman degradation data. Furthermore, the sequencing of amino acids was also increasingly made automated later in the 1960s. These innovations assisted the creation of the first published protein sequence database [7] in 1965.

Following Figure 1.1 further into the 1960s, researchers discovered the evolutionary value of having protein sequence data of different species. The problem to be solved back then was the quantification of the similarity between sequences. Pairwise alignment algorithms such as the algorithm of Needleman and Wunsch for global alignments [9] and that of Smith and Waterman for local alignments [11] from the 1970s solved this issue and alignment is still considered to be a key bioinformatics task to this day. Together with alignments, mathematical frameworks for amino acid substitutions in the context of evolution such as PAMs and BLOSUMs also contributed

to bioinformatics. These pairwise alignment algorithms are sufficient for comparing two sequences but unfeasible for searching databases for homologous sequences, hence faster algorithms like FASTA [12], Basic Local Alignment Search Tool (BLAST) [19] were developed in the 1980s and 1990s. These methods were and are still important for discovering functional, structural and evolutionary information in biological sequences since sequences demonstrating homology, or similarity due to shared ancestry, are highly likely to possess the same biological function. This also means that such sequences might be derived from a common ancestor and it became commonplace that sequence patterns may lead to structural and functional relevance. A natural extension of pairwise alignments is multiple sequence alignment (MSA) [20], which concerns aligning multiple related sequences. The most popular and still widely used tools today include Clustal [21] and MUSCLE [22]. MSAs reveal much more information than pairwise alignment can. They allow for the identification of conserved sequence patterns and critical amino acid residues with much more statistical significance which is of great value for constructing phylogenetic profiles of gene families [23]. All of this showed the importance of computational biology and established bioinformatics as a beneficial field of science.

Development of DNA-based applications took some more time since the genetic code and how it translates to amino acids was not deciphered yet until 1968 [8]. Early DNA and RNA sequencing methods were first demonstrated in the 1970s [10, 24] and like with protein sequencing methods, these methods only became faster, more efficient and more scalable. The 1990s saw the appearance of whole genome sequencing and internet-accessible databases that we still use to this day, such as Genbank [25], Ensembl [26] and the European Nucleotide Archive (ENA) [27]. This led to significant advancements in computational biology, driven by the continuous increase in data volume and the escalating demand for computational processing power. With the advent of second-generation sequencing in the 2000s came even more Big Data issues, further challenging bioinformaticians by allowing us to sequence millions of DNA and RNA base pairs in a single run. The sheer size and complexity of biological data can make it difficult to store and manage, as for instance implementing error identification, security, quality standards and easy data retrievability. On top of that, the analysis of such large-scale data is not straightforward and traditional software tools won't be sufficient anymore. Lastly, the need for high-performance computing resources to handle all of these computational demands will only rise.

Today we see that research in the field of biology is becoming more and more computationally driven and that this trend will not slow down any time soon [28]. This thesis will specifically concentrate on the role of computational approaches in protein research, which is detailed in the subsequent section.

1.2 Protein biology

Proteins are an essential part of molecular biology and are involved in almost all cellular functions. They are part of the essential biological macromolecules that make up life, hence a lot of effort has gone towards trying to understand the functions of protein and disruptions in its mechanisms that lead to many kinds of diseases. Proteins are composed of a linear chain of amino acids (AA) with a length ranging from 50 to tens of thousands of AAs, all connected by peptide bonds into a polypeptide. This is also referred to as the *primary structure* of a protein as mentioned earlier [17]. A sequence of amino acids is mostly determined by the genetic code without considering post-translational and post-transcriptional modifications etc. In the genetic code of all living organisms, there are 20 different kinds of amino acids coded in that make up the 'language' of proteins. Each amino acid has the same backbone but differs by the chemical properties of its side chain, also known as the R-group. This sequence of amino acids does not occur as a mere linear chain of peptides and consists of much more intricacies. The protein's *secondary structure* is formed by locally folded structures in the polypeptide chain, excluding the R-group. This folding is caused by chemical interactions within the backbone. The most common and well-known examples of these structures are the α-helices and β-sheets. The overall three-dimensional structure that forms out of these structures is referred to as the *tertiary structure*. These are formed due to interactions between the R-groups and are much harder to classify due to the quasi-infinite amount of potential conformations that could occur in a protein structure [29]. And lastly, a protein can also be made up of multiple polypeptide chains, referred to as its subunits. These subunits together form the *quaternary structure* of a protein.

The sought-after biochemical and cellular functions of a protein emerge from a combination of all of these structures. While a protein's 3D structure and function are dynamic and dependent on its surroundings such as the cellular

state and other proteins and molecules, it is still defined by its underlying sequence. This means that a lot of the 3D-structural and functional information of a protein should be retrievable from its amino acid sequence [30]. Understanding how a protein's sequence translates to its structure and function, otherwise known as the 'protein folding problem', is the central problem of protein biology and is crucial for understanding disease mechanisms and designing proteins and drugs for therapeutic and bioengineering applications. Therefore, a lot of effort has gone into computational methods for structure and function predictions from protein sequences but this sequence-structure-function relationship continues to challenge bioinformaticians. In the remainder of this chapter, we will discuss state-of-the-art bioinformatics methods to obtain more knowledge in this field.

1.3 Computational approaches to understand protein biology

State-of-the-art approaches

As mentioned earlier, the Edman degradation method was mostly used before to determine the primary structure of a protein. The current state-of-the-art methods for the identification of protein sequences are *de novo* sequencing algorithms applied to tandem mass spectrometry data [31] and allow simultaneous sequencing of thousands of proteins per given sample. Plenty of valuable biological and evolutionary information is already retrievable from just the primary structure *via* traditional tools such as BLAST and MSA as discussed earlier and could provide more information for the prediction of secondary and tertiary structures. However, to cope with the number of recorded protein sequences rising exponentially, far more compute-efficient methods based on multiple sequence alignments had to be developed like PSI-BLAST [32], HHblits [33] and MMseqs [34]. However, it's important to note that these methods might struggle to handle the continuously growing number of protein sequences stored in databases. As illustrated in Figure 1.2b, the UniProt Archive (UniParc) has seen a significant increase in recorded protein sequences, with the count now exceeding half a billion.

At the other end of the spectrum, the most common way to determine the 3D structure of a protein has remained to be X-ray crystallography for more

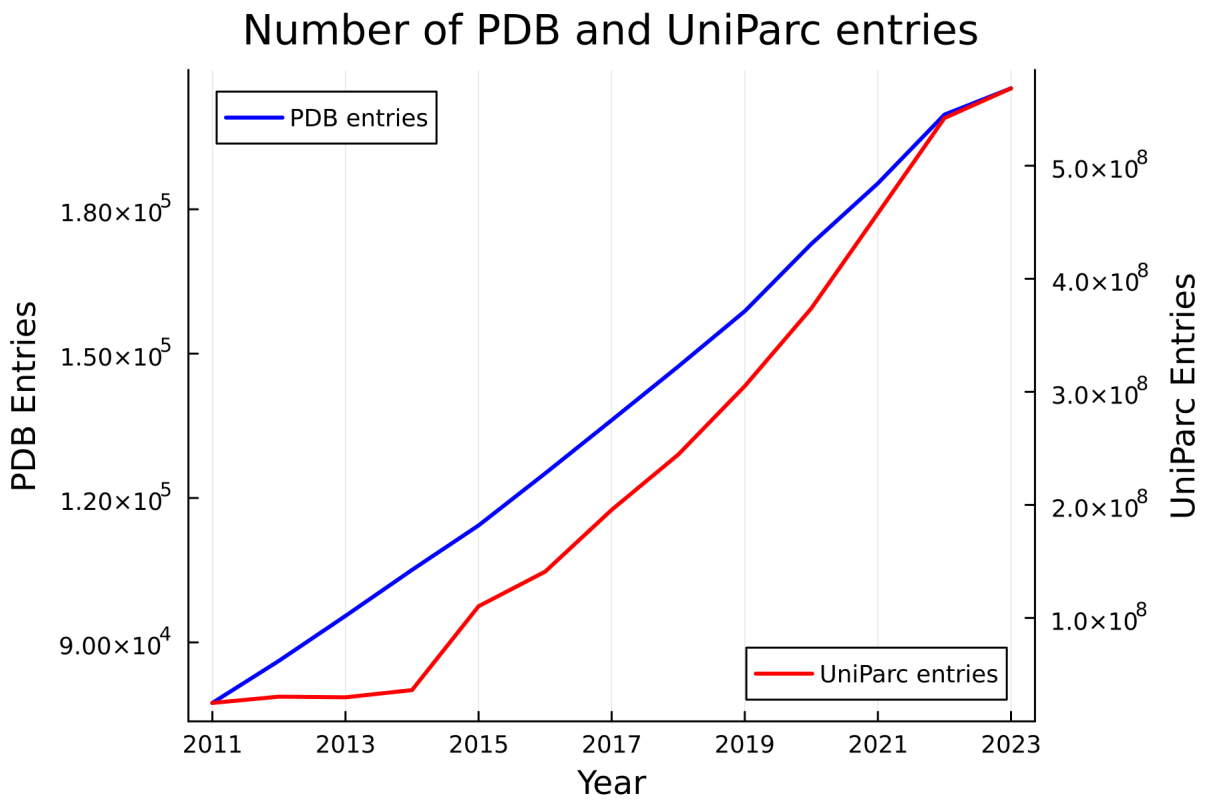

Figure 1.2: Total number of entries in PDB [35] in blue and the total number of entries in UniParc [36] in red, from 2011 to 2023 as of May 2023. Note the different scales.

than half a century [16], with cyro-electron microscopy now catching up rapidly [37]. However, these kinds of laboratory approaches for structure determination of proteins are complex, expensive and in some cases not possible for the protein in question whilst sequence determination is relatively much easier to perform. Because of that, the structures and functions for a large fraction of the approximately 20000 known human proteins remain unknown [38]. When we look at Figure 1.2 and compare the number of entries in the Protein Data Bank (PDB)[35] - a key database for protein structures - with the number of protein sequences in the UniProt Archive (UniParc) [36], it becomes clear that the growth of the number of verified three-dimensional structures in protein databases is not keeping up with the rapid increase in sequence information. This growing gap highlights the increasing importance of computational models that can predict protein structure and function.

A lot of methods have been developed to tackle this problem. Until recently, these methods were mainly based on statistical sequence models or physics-based structural simulations. *Ab initio* physics-based approaches such as ROSETTA [39] solve this problem by searching the protein's conformational space using atom energy functions and minimizing the total free

energy of the system. ROSETTA has shown to be effective at predicting unknown structures and has been widely used for varying applications, but also assumes simplified energy models, is extremely computationally intensive and has limited accuracies [40]. Statistical sequence modeling of a set of related proteins, on the other hand, has proven to be very useful for discovering evolutionary constraints, homology searches and predicting residue-residue contacts. Improvement of these models has mainly been data-driven; exploiting databases to build large deep learning systems which culminated in the recent success of DeepMind's AlphaFold2 [41] at the Critical Assessment of Protein Structure Prediction (CASP) 14. This success of AlphaFold continued into more recently CASP 15 [42]. Even though, DeepMind did not participate, the most successful participants integrated AlphaFold into their methods. However, all of these models are supervised methods that require labels. Labeled protein structure data essentially means retrieving the 3D coordinates of every atom in a protein which is very labor-intensive and time-consuming. Also, such kind of models would likely perform poorly when working with completely unrelated proteins since the model won't be trained on this kind of data.

One underlying theme of these computational methods for protein structure prediction is being able to translate the protein 'language' into numerical representations which computers can learn from. This is now known as the field of protein language modeling.

Protein language modeling

It is intuitive to represent a protein as a sequence of letters with each letter corresponding to an amino acid. As with natural languages, we can find common elements between naturally evolved proteins. Noticeable patterns reoccurring in multiple (related) protein sequences are highly likely to be biologically relevant. These motifs and domains are essential to many biological processes and can easily be represented as words, phrases or sentences of amino acids in a language model perspective. This is why researchers are taking inspiration from the recent successes of natural language processing (NLP) and applying this to a biological context. NLP is a branch of artificial intelligence (AI) concerning itself with creating the ability for computers to learn and understand (human) languages by using statistical, machine learning and in recent years deep learning models [43]. Common tasks in NLP include part-of-speech tagging (grouping words based on their function

in a sentence), named entity recognition (recognizing specific entities in a sentence such as locations, persons, dates etc.) and natural language generation (letter/word prediction).

As with protein language modeling, applying labels to millions of natural language data such as web pages, articles, journals etc. is a labor-intensive procedure and thus state-of-the-art NLP models use a form of *self-supervised learning*, a form of unsupervised learning in which the context of the text is learned to fill in missing words, predict the next word in a sentence etc. during the training as shown in Figure 1.3. This masked learning paradigm involves tokenizing input text into smaller units and converting them into numerical representations, followed by random masking of a certain percentage of tokens in the input sequence. The masked input sequence is then fed through multiple layers of a neural network architecture, which capture different levels of semantic and syntactic information, resulting in contextualized embeddings [44]. Finally, the model can be fine-tuned on a specific task using supervised learning. Through self-supervised masked learning, language models can learn a wide range of linguistic patterns and structures, enabling them to generate meaningful text, answer questions etc. The principles of self-supervised learning and masked learning from NLP can be adapted to the "language" of proteins to learn how a protein sequence translates to a three-dimensional structure [40].

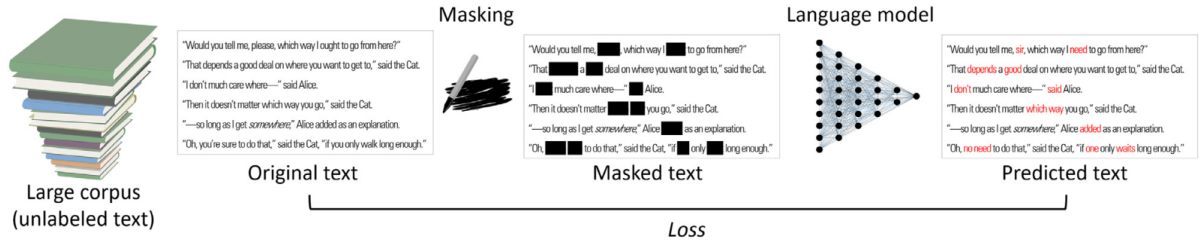

Figure 1.3: Demonstration of a self-supervised masked language learning model. A fraction of the unlabeled text is masked randomly and the language model will attempt to predict these masked tokens. The loss function is a method to assess the performance of the model on its predictions

Well-known NLP methods which adapt some kind of self-supervision include bi-directional long-short term recurrent neural networks (biLSTMs) such as ELMo [45] and more recently transformers such as Google's BERT [46] and OpenAI's GPT-3 [47] and GPT-4 [48]. Despite the simplicity of the idea behind self-supervision, such models pre-trained at scale have shown interesting capabilities with very little training on a specific task, now mostly referred to as *few-shot learning* [40].

In recent years, transformers have become the backbone of many state-of-the-art NLP and protein language models. Transformers are a class of neural network architectures that have revolutionized the field of natural language processing (NLP) since their introduction by Vaswani *et al.* in 2017 [49]. The key innovation of transformers is the self-attention mechanism, which allows the model to weigh the importance of each input token in relation to the others, enabling the efficient handling of long-range dependencies in text. Similar to NLP tasks, protein language models can be pre-trained on large-scale unlabeled protein sequence databases, to learn general features of protein sequences in an unsupervised manner. These pre-trained models can then be fine-tuned on specific protein-related tasks with limited labeled data.

State-of-the-art protein models leverage other advanced machine learning techniques to capture complex patterns in amino acid sequences and predict protein properties. These models employ a combination of sequence alignments, evolutionary information, and NLP-inspired transformer-based architectures to achieve remarkable performance in predicting protein structures and function with the most notable latest projects being TAPE [50], ProtTrans [51] and Meta AI's ESM-2 [52], one of the most recent and largest protein language models to ever have been developed at the time of writing. ESM-2 has been shown to accurately capture evolutionary information and to perform well on structure prediction tasks. It consists of transformer-based protein language models with up to 15 billion parameters trained on 65 million unique sequences.

As with natural language models, a consistent trend has been observed in protein language models wherein increasing the number of parameters and the amount of training data leads to ever-increasing performance. Remarkably, performance does not appear to saturate even with the largest models [43]. However, the computational power required to train such models and perform predictions with them grows exponentially with the number of parameters, reaching a point where modern computers struggle to keep up in a sustainable manner. For instance, training the 175 billion parameter GPT-3 model with 300 billion tokens is estimated to take at least 34 days using 1024 NVIDIA A100 GPUs [53]. While these advancements in computational modeling are undeniably impressive, they come with significant environmental costs in terms of energy consumption and material resources required to support such systems. While the specifics of the infrastructural requirements behind large-scale protein and natural language

models, including applications like OpenAI's ChatGPT, aren't typically made publicly accessible, we can still make some educated guesses about their environmental impact. For instance, it's estimated that the carbon emissions produced during the training process of GPT-3, the model underlying ChatGPT, amounts to 552 tonnes of CO_2 [54]. To put this into perspective, it is equivalent to the yearly carbon footprint of nearly 60 average Belgian residents [55]. Even with the vast computational requirements and their consequential environmental impact, it is important to not lose sight of our wider responsibilities in the realm of scientific research. As researchers continue to research natural language processing and protein language modeling, it is crucial to balance the pursuit of ever-larger models with the objective of sustainable and responsible development.

1.4 Goals and objectives

After a historical overview of bioinformatics and in particular protein research, we raised the issues in the current landscape of protein language modeling and its need for more computationally and data-efficient methods. In response to this need, we look to hyperdimensional computing. This computing paradigm, summarized by P. Kanerva [56], is inspired by the human brain's learning and adaptability capacities and provides an ultra-efficient and robust learning framework. The principal aim of this study is to explore the potential of hyperdimensional computing in protein sequence research, particularly focusing on the encoding of amino acids and protein sequences, evaluating their effectiveness in prediction tasks and understanding the performance and challenges along the way.

In the next chapter, we aim to provide an introduction to hyperdimensional computing, allowing the reader to gain an understanding of its underlying principles, operations and its potential for applications in the realm of bioinformatics and protein research by demonstrating its operations and applying them in small-scale examples.

In Chapter 3, the objective is to investigate and formulate strategies for encoding amino acids and protein sequences whilst leveraging the potential of hyperdimensional computing.

In the chapter thereafter, we aim to apply the developed encoding methods to a protein sequence database, PhaLP, a specialized resource for phage

lytic proteins developed by Criel *et al.* [1]. Additionally, we plan to utilize the encoded sequences and the data of PhaLP as input information for classification tasks, experimenting with a variety of learning methods, whether or not based on hyperdimensional computing, to evaluate the effectiveness of our hyperdimensional embeddings in prediction tasks.

Lastly, in Chapter 5, the objective is to utilize hyperdimensional and context-aware amino acid representations as input information for amino acid-level prediction tasks to discover potential avenues for designing computationally efficient alternatives to state-of-the-art protein language models.

2. HYPERDIMENSIONAL COMPUTING

Hyperdimensional computing (HDC) is a relatively recent paradigm of computing in which data is represented and manipulated by high-dimensional (or hyperdimensional) vectors in the range of tens of thousands bit. This framework, outlined by Kanerva [56], is inspired by the workings of the human brain and its ability to adapt, learn fast and easily understand semantic relations. The human brain consists of about 100 billion neurons (nerve cells) and 1000 trillion synapses that connect these neurons. Each neuron is connected to up to 10,000 other neurons, creating massive circuits. This is likely fundamental to the workings of the human brain and what separates our brains from modern von Neumann computer architectures, which operate on 8 to 64-bit vectors. This becomes clear when we compare the relative simplicity for a human to learn a language compared to computers. Computers use a large and complicated set of arithmetic operations in the form of deep learning networks, which require terabytes of data and thousands of Watts of computing power to come close to mastering a language whilst a human can recognize other languages relatively easily when they don't even speak it. Likewise languages, we can very easily memorize and compare other intrinsically complex and contextual concepts such as images. A computer would have a hard time finding similarities between a set of images and faces because this requires very complex machine learning models. The human brain can do this all with a very large efficiency by consuming only roughly 20 W of energy.

Achieving these kinds of flexible brain-like models based on high dimensionality is not entirely new and is being explored since the 1990s. Some of these earlier models include Holographic Reduced Representations [57], Spatter Code [58] and others. A hyperdimensional vector (HDV) can represent anything from a scalar number to any kind of concept. This vector is initially made up of totally random elements, but with a simple set of operations, which will be explained later, we can use other vectors to combine some concepts into new similar or dissimilar concepts. For example, to show

the essence of HDC and how it tries to simulate the brain, we can compare the concept of a *table* to the concept of a *brocolli*. We would not immediately conclude that they are in any way similar but as humans, we can trace back *table* to *plate*, which has some similarities with *food* from which we can easily extract the concept of *brocolli* as in equation 2.1. These kinds of operations are not very obvious for a classical computer but creating these semantic pathways and recognizing links between distant objects are rather easy for humans. Two unrelated concepts are noted by $\neq$ and two related concepts by $\approx$.

$$\begin{aligned} &\text{table} \neq \text{brocolli} \\ &\text{table} \approx \text{plate} \approx \text{food} \approx \text{brocolli} \end{aligned} \tag{2.1}$$

The elements in an HDV can be made up of binary bits (values from the set 0, 1) like in classical computing but also of bipolar (values from the set -1, 1) or real numbers. The choice of the nature of the elements has also implications on the nature of the different operations and possibly the results.

An initial HDV is generated randomly. This *holistic* or *holographic* representation of a concept spread out over a vector consisting of thousands of bits gives rise to interesting properties such as its robustness agaisnt noise [59]. These kinds of systems are very tolerant to noise and failure of bits since we introduce a lot of redundancy in the vector just by stochastics. This is very unlike classical computing where every bit counts and one failure in a bit can lead to immediate data corruption. Besides its robustness, it also has the potential to perform much faster and more efficient computations than traditional computer systems since it allows for more efficient data storage by encoding multiple objects into a vector [56][59].

2.1 Operations on hyperdimensional vectors

The interesting properties of HDC are based on only four basic operations we can perform on HDVs. We will discuss these for bipolar and binary vectors. From here, all implementations are written in the programming language Julia [60] unless noted otherwise. Known for its efficiency, Julia's blend of high-level, interpreter-based features makes it possible to write powerful programs. This is particularly beneficial when working with high-dimensional spaces. Julia's built-in support for bitvectors and bitmatrices, along with

parallel computing, will be useful for this thesis. Furthermore, the lively Julia community supports a rich ecosystem and a broad array of packages to utilize.

Before the operations are demonstrated, we show how a random hyperdimensional vector can be generated in Julia. In the following code block, functions to generate binary and vectors can be made effortlessly with one line each.

```
# Built-in package for random number generation
using Random

# Binary HDV
bithdv(N::Int=10_000) = bitrand(N)
#Bipolar HDV
hdv(N::Int=10_000) = rand((-1,1), N)
```

Bundling

Also referred to as *superposition* or *aggregation*, the element-wise addition as in equation 2.2 of n input vectors $[X_1 + X_2 + \cdots + X_n]$ creates a vector X that is similar to the input vectors.

$$X = [X_1 + X_2 + \cdots + X_n] \tag{2.2}$$

For bipolar vectors, this entails a straightforward element-wise addition. The resulting vector is restricted to a bipolar nature too depending on the sign of each element, thus containing only -1, 1 but allowing 0 for elements that are in disagreement as shown in the following 6-dimensional example.

$$\begin{array}{rcccccc}
X_1 = & +1 & -1 & +1 & +1 & -1 & -1 \\
X_2 = & +1 & +1 & +1 & -1 & -1 & -1 \\
X_3 = & -1 & -1 & +1 & +1 & -1 & +1 \\
X_4 = & -1 & -1 & -1 & +1 & -1 & +1 \\
\hline
[X_1 + X_2 + X_3 + X_4] = & 0 & -1 & +1 & +1 & -1 & 0
\end{array}$$

For binary vectors, the vectors are element-wise bundled based on the majority element. This is no problem if an odd number of input vectors are

considered but ambiguity rises when bundling an even set of vectors. This can be solved by setting the element in question randomly. [61] Another possibility is to add another random vector however this may seem to add more unnecessary noise, especially when bundling a low number of vectors. We can also reverse this by an *inverse addition*. For bipolar vectors, this means just multiplying the vector of interest by -1. A binary vector can be flipped bit-wise. These kinds of operations are not directly built into Julia, but are easily programmed as followed:

```
# Adds bitvectors element-wise based on the majority element.
# Random if tied.
# Reduce function takes another function (here .+)
# and applies it to all given vectors.
# 'Dotted' operations such as .+ are vectorized
# making it element-wise.
function bitadd(vectors::BitVector ...)
    v = reduce(.+, vectors)
    n = length(vectors) / 2
    x = [i > n ? 1 : i < n ? 0 : rand(Bool) for i in v]
    return x
end

# Adds bipolar vectors element-wise and rounds off to -1,0 or 1
# depending on the resulting sign.
add(vectors...) = reduce(.+, vectors) .|> sign
```

Similar to an ordinary arithmetic summation, the bundling addition of hyper-dimensional vectors is commutative so the result is not dependent on the order of addition.

$$[X_1 + X_2] = X = [X_2 + X_1] \tag{2.3}$$

Binding

Two vectors can be multiplied element-wise resulting in a vector maximally dissimilar to the input vectors. Vectors X and Y are bound together forming Z being orthogonal to X and Y as shown in equation 2.4.

$$Z = X \circ Y \tag{2.4}$$

This *binding* operation translates to a simple arithmetic element-wise multiplication for bipolar vectors. For binary vectors, this is represented by a *XOR* bit-operation shown as follows.

$X =$	1	0	1	1	0	0
$Y =$	1	1	0	1	0	1
$X \circ Y =$	0	1	1	0	0	1

In Julia, there is a built-in function to carry out bit-operations such as *XOR*. For bipolar vectors, a simple element-wise multiplication suffices.

```
# Bind binary vectors
bitbind(vectors::BitVector ...) =  reduce(.xor, vectors)

# Bind bipolar vectors
bind(vectors...) = reduce(.*, vectors)
```

The binding operation can also be undone by multiplying with the same vector again. It is its own inverse so that:

$$A \circ A = O \tag{2.5}$$

Where O is a vector containing only zeros. Likewise an ordinary multiplication, this operation is commutative and distributive over additions, meaning that transforming a bundle of concepts with binding is equivalent to binding every element before bundling.

$$A = Z \circ (X + Y) = X \circ Z + Y \circ Z \tag{2.6}$$

Permutation

The permutation operation of an HDV, is a reordering of the contents of the HDV. This can be random but a circular shift is widely employed [62] and makes the operation easily reversible. This results in a vector technically dissimilar from the input vector but still encoding its information. This will become important later when it will be used to encode sequential informa-

tion such as tokens in a text. This operation will be denoted by Π.

$X =$	1	0	1	1	0	0
$\Pi(X) =$	0	1	0	1	1	0

In Julia, this line can do it for both binary and bipolar vectors:

```
# Permute by applying a circular shift
perm(vector::AbstractVector, k::Int=1) = circshift(vector, k)
```

Similarity measurement

For many kinds of problems, it will be necessary to quantify the similarity between two HDVs. The method depends on the nature of the vectors. For binary vectors, the *Hamming distance* defined as:

$$\text{Ham}(A, B) = \frac{1}{d} \sum_{i=1}^{d} 1_{A(i) \neq B(i)} \tag{2.7}$$

The *cosine distance* as defined in equation 2.8 is most commonly used for bipolar vectors:

$$cos(A, B) = \frac{A \cdot B}{||A|| * ||B||} \tag{2.8}$$

Both are not built-in Julia by default, but can be programmed as followed:

```
# Built-in package for linear algebra operations
using LinearAlgebra

# Hamming distance
hamming(x::BitVector, y::BitVector) = sum(x .!= y)/length(x)

# Cosine similarity
cosine(x::Vector, y::Vector) = dot(x, y) / (norm(x) * norm(y))
```

The results of both of these measurements are summarized in table 2.1.

It is important to note that two random HDVs will be quasi-orthogonal to each other just by stochastics. Also notice that the first quantifies a distance and the latter a similarity.

Table 2.1: Overview of similarity measurements in HDC depending on the nature of the HDVs

Measurement	Dissimilar	Orthogonal	Similar
Hamming distance	1	0.5	0
Cosine similarity	-1	0	1

2.2 Examples

There are many interesting possibilities given the relative simplicity of all these operations. In this section, we will demonstrate the power of hyperdimensional computing with some simple examples.

Simple example with simulated data

To get a feel for the operations, assume A, B, C, X, Y and Z to be random 10,000-dimensional bipolar hypervectors and that $D = X \circ A + Y \circ B + Z \circ C$, let us then try to retrieve A from D by using the defined operations. We generate for A, B, C, X, Y and Z each a random 10,000-D vector. To retrieve an approximation of A, D can be multiplied by X and the rest of the included vectors are then regarded as noise as done in equations 2.9. Because of the robustness of hyperdimensional vectors, a lot of information of A should still be contained within D.

$$\begin{aligned} A' &= X \circ D \\ &= X \circ (X \circ A + Y \circ B + Z \circ C) \\ &= \underbrace{X \circ X \circ A}_{A} + \underbrace{X \circ Y \circ B + X \circ Z \circ C}_{\text{noise}} \\ &\approx A \end{aligned} \tag{2.9}$$

The procedure of equation 2.9 is repeated 10,000 times because of the stochastic nature of these vectors. The results are illustrated in figure 2.1. We see that we can retrieve a lot of information with most of the Hamming distances centering around 0.25. Due to the high-dimensional space and thus its robustness, the distances are very consistent. Notice that two completely random HDVs would have a distance close to 1 just by stochastics. A Hamming distance of 0 would mean that we retrieved all bits of A correctly, which is impossible in this model due to the consideration of noise. Although we work with a very constrained model, vector A is roughly 75 % retrievable

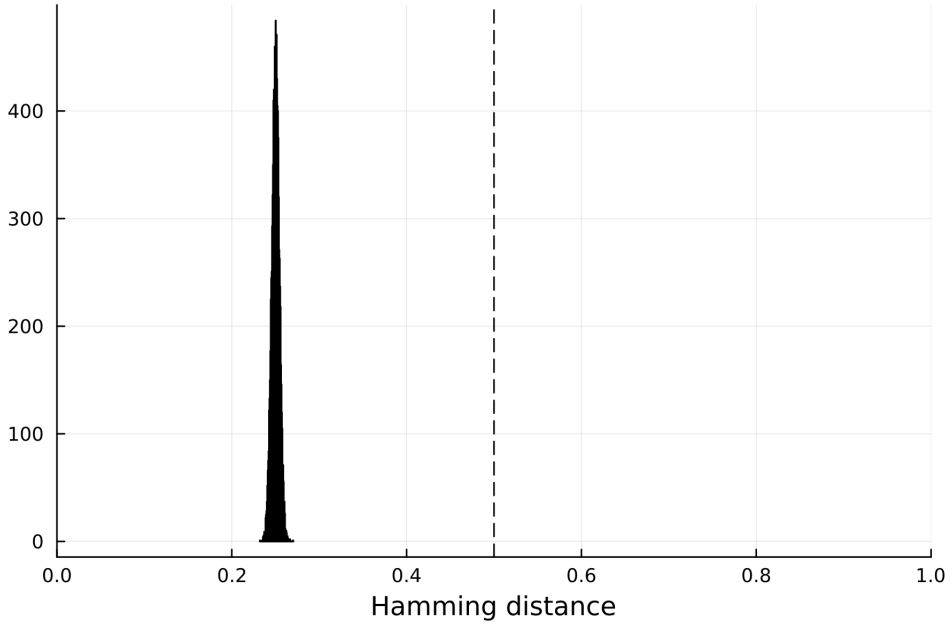

Figure 2.1: 10,000 cases of random 10,000-dimensional binary vectors being made by equation 2.9. The resulting Hamming distances between A and A' are then plotted in a histogram. Dashed line indicates a Hamming distance of 0.5, meaning that two vectors are orthogonal.

and the calculations are very efficient as all of these can be completed in less than 2 seconds on a laptop. This same experiment was done with random bipolar, 10,000-dimensional vectors and it performs slightly slower as expected but retained the accuracy.

2.3 Examples of hyperdimensional computing with real datasets

Now, the power of these simple operations will be demonstrated by applying them to a couple of relatively small real datasets.

Zoo animal classification

As the first example, we will consider a simple dataset containing 101 animals with 17 descriptors such as their number of legs, their skin covering and other physical properties [63]. Our goal is to create a simple model that can classify these animals and other animals that are not present in the dataset based on their descricptors. To tackle this problem, we first assign to each descriptor a random hyperdimensional vector. For each animal, all of

its features can be bundled to obtain a final vector representing the animal. For example, it is known that a chicken lays eggs, is covered with feathers and has two legs so then these features can be bundled as in the following equation. C is a vector representing a chicken, E the ability to lay eggs, F the possession of feathers and T the possession two legs:

$$C = E + F + T \tag{2.10}$$

This is simple for all the variables that have binary values, but the feature for the number of legs is variable. Although it is possible to assign completely random vectors to each number of legs, it would make a slightly more biologically realistic model if an animal with 2 legs would be more similar to one with 4 legs than to one with 8 legs. To address this, a range of numbers would have to be representable by hyperdimensional vectors, the range from 0 to 8 in this case. First, a random hyperdimensional vector representing the lower bound of the interval is generated. Next, a vector representing the next step in the interval is constructed by replacing a fraction of the vector with random bits. This last step is then repeated to obtain a vector of each number in a range.

In biology, it is possible to find higher-order of concepts that are combinations of directly observable characteristics. For example, an animal could lay eggs or be dependent on its mother's milk, but (almost) never both. So, the growth and development of an animal depend on these characteristics. This property can be easily implemented into this HDC model by binding an HDV of a higher order concept to the descriptor HDV. So as said previously, the 'milk' (M), and 'egg' (E) features yields information about the growth of the animal, so we will create another vector representing the growth feature (G) to obtain a more expanded model. This is also done for the skin protection features (S) and all the features considering the limbs (L). This also gives us the possibility to retrieve some features of the animals as in the procedure shown in the previous example. Thus, equation 2.10 can be expanded into:

$$C = G \circ E + S \circ F + L \circ T \tag{2.11}$$

After conducting the various procedures, the data set now consists of 101 animals, each represented by a 10,000-dimensional feature vector. To efficiently analyze and visualize this high-dimensional data, principal component analysis (PCA) has been employed to reduce the dimensionality from

10,000 to just two. By projecting these vectors onto a 2D space, the data can be conveniently displayed in a two-dimensional plot, as illustrated in Figure 2.2. Upon examination of the plot, three distinct and meaningful clusters of animal classes emerge, which align well with our understanding of evolutionary relationships. These clusters include: (1) mammals, (2) a group consisting of birds, reptiles, and amphibians, and (3) a cluster encompassing invertebrates and insects. While the current analysis already provides valuable insights into the relationships between different animal classes, further improvement could be achieved by incorporating additional features that may lead to a clearer separation of these groups. By doing so, the model would be able to more accurately distinguish between the different animal classes and provide a more comprehensive understanding of their evolutionary connections.

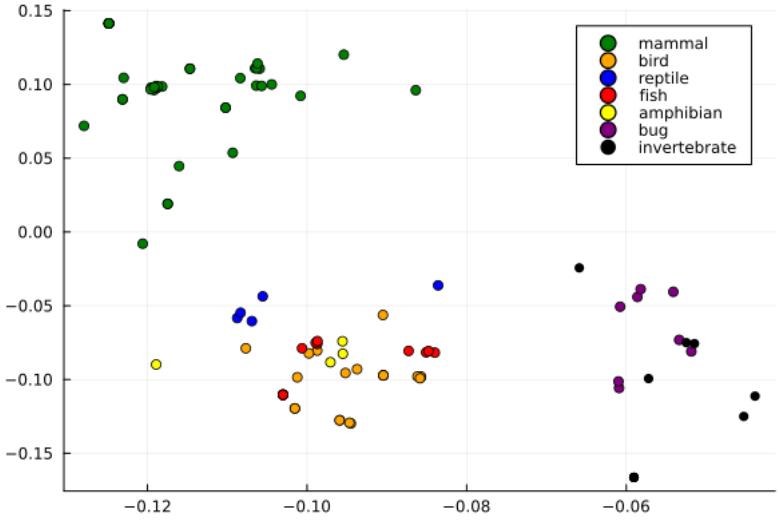

Figure 2.2: Scatter-plot of the first two principal components (PCs) of a 101×10,000 matrix containing hyperdimensional vectors for every animal in the zoo dataset after a PCA procedure. These PCs account for roughly 48 % of the variance.

After an HDV has been made for every animal, all animals of the same class can be bundled to obtain an HDV representing the said class. So for example, if we have a hyperdimensional vector for a pigeon (P), chicken (C) and a kiwi (K), an HDV representing birds (B) can be made by doing:

$$B = [P + C + K] \tag{2.12}$$

To classify an animal, its HDV can be compared to the HDVs of every class and the most similar vector is then assumed to be its class. In the following code block, the hypervectors for every animal and class have been already made as discussed above. The resulting HDV for a flamingo has been com-

pared to every other class vector *via* a measurement of the Hamming distance. The distance of flamingo HDV to the bird HDV is significantly smaller than to all other vectors

```
# HDVs for every animal class HDVs have been made already
# Take flamingo HDV out of dataframe
flamingo = data.species_hdv[24]
println("Hamming distance to mammal = ",
hamming(flamingo, mammal))

println("Hamming distance to bird = ",
hamming(flamingo, bird))

println("Hamming distance to reptile = ",
hamming(flamingo, reptile))

println("Hamming distance to amphibian = ",
hamming(flamingo, amphibian))

println("Hamming distance to bug = ",
hamming(flamingo, bug))

println("Hamming distance to fish = ",
hamming(flamingo, fish))

println("Hamming distance to invertebrate = ",
hamming(flamingo, invertebrate))

# Output
# Hamming distance to mammal = 0.303
# Hamming distance to bird = 0.1044
# Hamming distance to reptile = 0.2727
# Hamming distance to amphibian = 0.313
# Hamming distance to bug = 0.2867
# Hamming distance to fish = 0.3484
# Hamming distance to invertebrate = 0.4061
```

For further improvement, it would be possible to generate a set of animals not present in the dataset and test those in order to further understand how

this model can be improved. On top of this, it would also be possible to generate a confusion matrix to understand where we could use more distinguishing descriptors. From the PCA, we could already predict that reptiles and amphibians would be easily confused, as for invertebrates and bugs.

Protein classification

To illustrate an example more akin to this research topic, a model based on the principles of hyperdimensional computing will be built to classify a protein sequence dataset [64]. It contains 949 manually curated peptide sequences with their membranolytic anti-breast cancer activity level (very active, moderately active, experimentally inactive and virtually inactive). The virtually inactive peptides are predicted to be inactive. The model will be built with mostly the same procedure as for the animal classifier, but instead of animals, sequences have to be encoded into HDVs now. First, a random HDV is generated for every amino acid. Physicochemical properties, evolutionary constraints etc. could be introduced to make this model more realistic but that is not necessary for this demonstration. Next, a peptide sequence is to be considered as a bag of trimers as seen in figure 2.3. A vector representing a trimer is generated by binding the three amino acids whilst retaining sequential information by shifting as in equation 2.13. All retrievable trimers from a given sequence are then bundled together, forming a vector representative of the sequence.

$$ABC = A \circ \Pi(B) \circ \Pi(\Pi(C)) \tag{2.13}$$

From here on, the same procedures as in the last example can be applied here too, so all HDVs of a class are bundled for further analysis. The PCA procedure did not generate interesting results because the two first principal components explained only 5 % of the variance. This means that it is not feasible to reduce the 10,000 dimensions of the vectors to two, likely because the information is too smeared out over the vectors. This occurrence is highly dependent on the training data. Nevertheless, this follows the philosophy of hyperdimensional computing in keeping holistic representations of concepts.

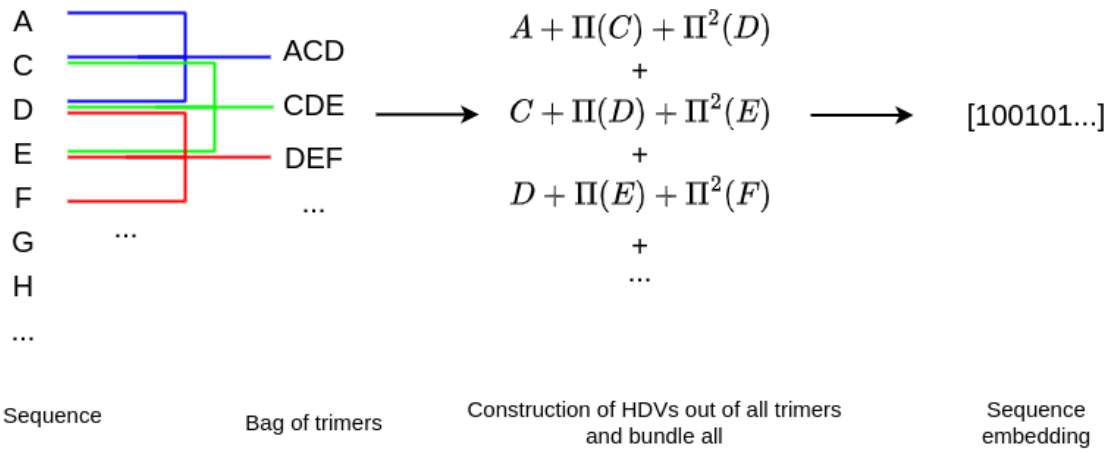

Figure 2.3: Overview of operations done to obtain an HDV of a protein sequence for the example concerning the real peptide dataset. First, a random HDV is generated for every amino acid. Next, a peptide sequence is to be considered as a bag of trimers. A vector representing a trimer is generated by binding the three amino acids whilst retaining sequential information by shifting as in equation 2.13. All retrievable trimers from a given sequence are then bundled together, forming a hyperdimensional vector representation of the sequence.

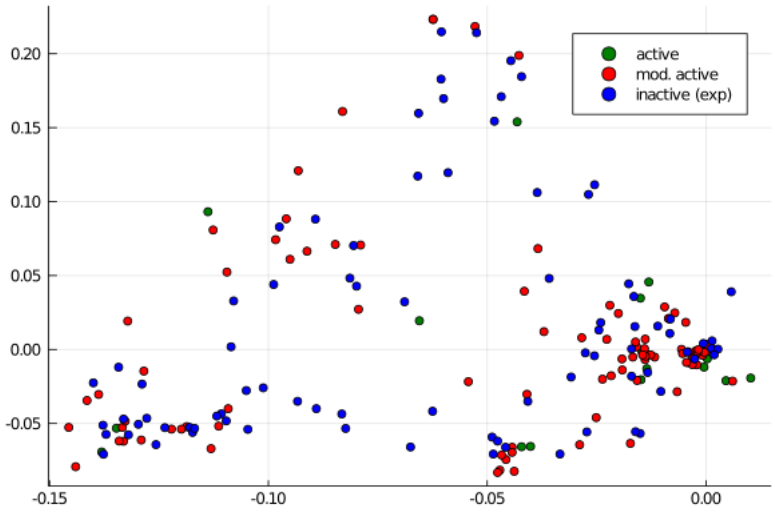

Figure 2.4: Scatter-plot of the first two principal components, projecting the 10,000-dimensional vectors for every peptide into the 2 main PCs. These PCs account for roughly 5 % of the total variance

Next, a classifier was made correspondingly. The dataset was stratified and split into a training set (comprising 80 % of the sequences) and a test set. With 100 runs, it could predict a protein sequence's class with an accuracy of 85 %. It has to be taken into account that the predicted inactive peptides account for 80 % of the sequences of the dataset, thus this model performs slightly better than if we would predict at random. There are many possible improvements to be made however, such as using more suitable

performance metrics, introducing similarities between amino acids instead of setting them randomly and using more suitable frameworks for our protein classification models, which will all be research topics further on in this project.

3. HYPERDIMENSIONAL COMPUTING METHODS TO ENCODE AMINO ACIDS AND PROTEIN SEQUENCES

3.1 Introduction

To research the possibilities of the hyperdimensional computing framework applied to protein language modeling, we introduce a rudimentary pipeline. First, amino acids have to be encoded into hyperdimensional vectors. Second, these vectors for every separate amino acid can be then further encoded into vectors representing a full protein sequence. And lastly, these embeddings could be then utilized to perform predictions such as classifications as shown in figure 3.1. The first two steps of this pipeline will be discussed further in this chapter.

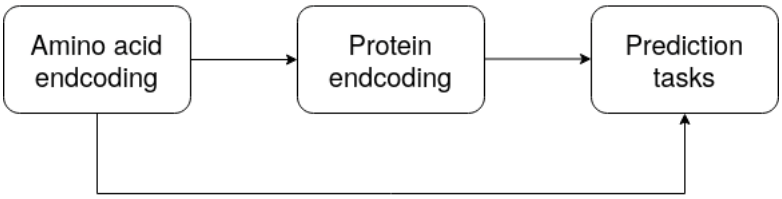

Figure 3.1: A simple demonstration of the proposed workflow. First, we encode individual amino acids into hyperdimensional vectors. With these, protein sequences could be encoded into hyperdimensional vectors. Lastly, both kinds of embeddings could be then used for prediction tasks.

3.2 Encoding single amino acids into hyperdimensional vectors

Currently, in most of the research in hyperdimensional computing, there is an emphasis on creating and assigning hyperdimensional vectors to certain concepts at random. This is useful for optimizing speed and efficiency and is not a problem for many prevalent research areas such as natural language processing, where, for example, it is typically assumed that a letter's similarity to other letters in the alphabet remains constant. However, the practical application of hyperdimensional computing to biological data remains limited at present, posing a challenge in extending its utility to this specific domain. Some notable studies include HDNA which assigns random hyperdimensional vectors to DNA bases to encode DNA sequences and BioHD [65] which encodes protein sequences using random mRNA hypervectors to use in genome sequence searches. In the context of DNA sequencing, the assumption of assigning random hyperdimensional vectors may not present as significant an issue as with proteins. This is largely due to the distinct nature of DNA bases as they do not display the same degree of physicochemical diversity that amino acids in proteins do. DNA bases serve primarily as the information carrier in the biological system, with their sequence dictating the sequence of amino acids in proteins. In this role, the relevance of their physicochemical properties to their informational role is rather limited in comparison to amino acids, which main function is to dictate the structure and function of the resulting protein. Whilst there are phenomena in DNA structures such as base stacking and hydrogen bonding that play a role, the simple base-to-vector mapping often suffices.

When considering protein language modeling, however, this assumption might be suboptimal since some amino acids are chemically more similar to each other than to others which is crucial to the protein's structure and function. We can already estimate physicochemical distances between amino acids based on their physicochemical properties [66] such as volume, polarity, chemical groups etc. *via* many kinds of distance measures. The different similarities between amino acids are tied into the structure and thus function of amino acid sequences and shape our view of protein language. It explains why some amino acid substitutions can result in almost no phenotypical changes or on the other hand detrimental changes. Proteins have evolved to maintain their structure and function, and dras-

tic changes in physicochemical properties can disrupt these characteristics. Therefore, amino acid substitutions that preserve the physicochemical properties of the original amino acid are more likely to be selected, resulting in a negative correlation with physicochemical distance. To account for this, we experimented with several methods to encode physicochemical distance into amino acid hypervectors.

Besides encoding amino acids as building blocks, it is also useful to encode amino acids in the context they are found in. State-of-the-art protein language models have the ability to gather information on long-range dependencies around a single amino acid and encode this information into neural networks and in dense numerical vectors. These models are very powerful, but, as discussed earlier, very resource-intensive as well. To investigate the possibilities of developing contextual embeddings on the level of amino acids, we propose a novel encoding technique within the hyperdimensional computing framework.

3.3 Encoding proteins into hyperdimensional vectors

Once hyperdimensional vectors are constructed for each amino acid, the next step is to combine these vectors to form representations of protein sequences. We can draw inspiration from the operations in hyperdimensional computing, which have already been applied in natural language processing. Similar to how characters are combined to form words and sentences, we can leverage similar principles to combine amino acids and generate meaningful representations of protein sequences.

In Section 2.3, we introduced the bag-of-words (BoW) method of embedding sequences in hyperdimensional space, which has been extensively applied to cases related to natural language processing in a hyperdimensional computing context. We also introduce a novel sequence embedding method in hyperdimensional computing.

3.4 Methods

From here on, every hyperdimensional vector is made to be 10,000-dimensional with randomly assigned binary elements unless noted otherwise.

3.4.1 Encoding single amino acids into hyperdimensional vectors

Projected ESM-2 embeddings

The last layer of the 3 billion-parameter ESM-2 model [52] of every amino acid was extracted, resulting in 1024-dimensional real-valued embeddings for every amino acid. To project these into hyperdimensionality, a simple matrix multiplication has been employed:

$$A \times B = C$$

Where A is a 1024-dimensional ESM-2 embedding and B a matrix of 1024 random 10,000-D vectors. The resulting vectors are then min-max scaled and rounded depending on the desired nature of the vectors. To visually assess these, the vectors for each amino acid are reduced in dimensionality *via* PCA into two dimensions. This has been compared to a PCA of the unaltered 1024-dimensional ESM-2 embeddings.

Real-valued projected ESM-2 embeddings

It is possible to step away from binary hyperdimensional vectors, which are typically used in hyperdimensional computing research, and allow the vectors to be real-valued. This gives us the possibility to store more data in a vector and utilize more complex mathematical operations with the cost of losing efficiency of bit-operations. We generated random real-valued vectors with random values in [-1,1]. Real-valued ESM-2 embeddings were generated by the same procedure as above, but without the rounding.

Enforcing similarities using genetic algorthims

Instead of utilizing embeddings coming from other large protein language models, we also experimented with encoding predetermined target pairwise distances onto initially random hyperdimensional vectors. First, a suitable matrix with predetermined pairwise distances has to be considered. This also implies that the matrix has to be symmetric. If we then consider the 20 essential amino acids, the problem at hand would involve a set of 20 binary vectors of length 10,000 to conform to a target distance matrix based on Hamming distance. This can be classified as a combinatorial optimization problem as it involves searching for an optimal or near-optimal configuration of binary vectors that satisfy a specific criterion. To minimize the difference between the target and actual Hamming distances for all pairs of binary vectors, we could adjust the vectors by randomly bit-flipping them until they meet the desired criteria. However, the search space in this problem is vast ($2^{10,000x20}$), making exhaustive search methods computationally infeasible. Thus, more efficient algorithms are needed to solve this problem such as genetic algorithms [67] (GAs). GAs, a subfield of evolutionary algorithms, draw inspiration from the process of natural selection and emulate the evolutionary mechanisms of crossover, mutation, and selection to explore a vast search space and converge toward an optimal or near-optimal solution. A genetic algorithm was implemented with the Evolutionary.jl package [68] in Julia to encode target similarities. The primary steps of a genetic algorithm include:

- Initialization: random candidate solutions are initiated with a given population size.
- Crossover: combine genetic material offspring of two parents (in this case vectors). There are many recombination techniques such as single-point, multi-point and uniform crossover.
- Mutation: randomly alterate genes (in this case bits) to explore other possibilities of configurations and prevent premature convergence due to local optima.
- Evaluation: Each individual in the population (in this case a set of vectors) is assessed using a fitness function, which measures how well the solution solves the given problem.

- Selection: individuals from the population are selected based on their fitness to create a mating pool. Fitter individuals have a higher probability of being selected, mimicking the concept of survival of the fittest in natural evolution.

These steps are reiterated over a number of generations to obtain a set of vectors that correspond to the best fitness. A BLOSUM62 substitution matrix [69] and Grantham's distance matrix [70] were considered as target pairwise similarity matrices for the GA. These were then normalized to obtain the target pairwise Hamming distances. The fitness is determined by the sum of the squared differences between the computed distance matrix of an individual and the target distance matrix. The lower the fitness value, the more optimal the individual. The population size was set to 25,000 and the number of generations to 250. The mutation rate was set to 0.15 and the crossover rate to 0.2, these are high and low respectively compared to more commonly used parameters because we want to emphasize the bit-flipping and avoid recombination of vectors for faster convergence.

Contextualized neighborhood-encoding of amino acids

To encode the neighborhood of an amino acid in a sequence, all possible pairwise interactions with the central amino acid in question in a given window are made *via* binding and then all encoded into one vector *via* bundling as shown figure 3.2. Our neighborhood-encoder was tested on the human reference proteome in UniProt, entry *UP000005640*, containing 20591 proteins. We started with real-valued random vectors and real-valued projected ESM-2 vectors for every amino acid. Windows of $n = 4$ and $k = 50$ were considered resulting in four different experiments. Every single residue in the human reference proteome was encoded with information within the k-range window and an average vector was made for every amino acid. For all 20591 peptides in the reference proteome, this procedure took only three hours for $n = 4$, but upwards to 15 hours for $n = 50$ on a high-performance computing cluster (HPC). After all amino acids were encoded, an element-wise average was made for every amino acid. The resulting hyperdimensional vectors were kept to a real-valued nature to not lose information for illustrative purposes. Principal component analysis was then done for these four experiments as seen in figure 3.6.

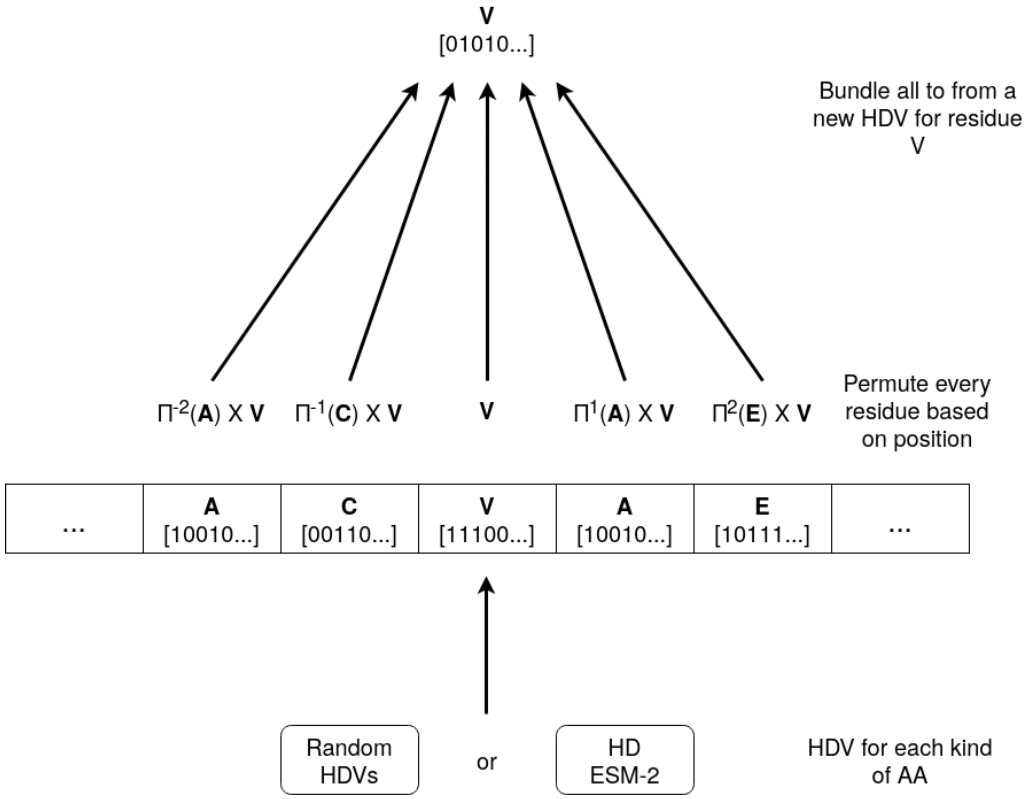

Figure 3.2: A simple demonstration of our amino acid encoder. First, HDVs are generated for every kind of amino acid, this can be done using just random HDVs, projected ESM-2 embeddings, GA-optimized vectors etc. It considers an amino acid and all amino acids in a predetermined neighborhood (here $n = 2$). It produces all possible interactions of the central amino acid in the window by binding and then bundles all the pairwise interactions into one hyperdimensional vector that represents the central amino acid.

3.4.2 Encoding proteins into hyperdimensional vectors

We implemented two different algorithms to encode amino acid vectors into vectors representing proteins. We already introduced the BoW-method in 2.3, fully explained in figure 2.3. We also introduce a novel sequence embedding method in hyperdimensional computing. It is similar to the bag-of-words method in the sense that it bundles vectors of k-mers, but here, the k-mer's positional information will be encoded into the k-mer by permuting it before bundling as seen in figure 3.3, similarly to how a convolutional layer in a neural network operates so we will name it the convolutional embedding method from here on. These methods will be extensively utilized and tested in chapters 4 and 5 where several case studies consisting of protein sequences datasets are tackled.

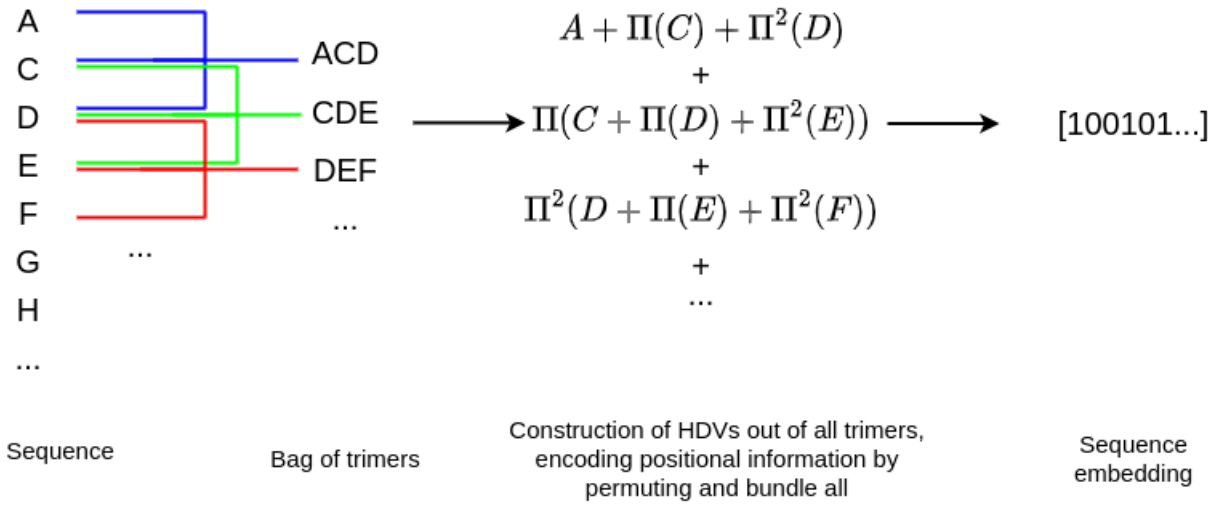

Figure 3.3: Overview of operations done to obtain an HDV from a sequence using the convolutional embedding method. First, an HDV is generated for every amino acid. Next, a peptide sequence is to be considered as a bag of trimers. A vector representing a trimer is generated by binding the three amino acids whilst retaining sequential information by shifting as in equation 2.13, just as in the BoW-method (figure 2.4). On top of that, every trimer will also be positionally encoded via a permutation operation. All retrievable trimers from a given sequence are then bundled together, forming a hyperdimensional vector representative of the sequence.

3.5 Results

3.5.1 Projected ESM-2 embeddings

Visually, no interesting patterns can be deducted from the PCA decompositions of the ESM-2 embeddings. Yet, if we also perform a principal component analysis on random vectors, we can see there is significantly more variance encoded into the first two principal components of the ESM embeddings (22 %) compared to random vectors (10.5 %, can deviate slightly depending on the run), meaning that there should be a significant amount of similarity encoded into the hyperdimensional vectors. PCA decomposition of our projected ESM-2 embeddings can't fully retrieve the variance in the hyperdimensional vectors as well as in the unaltered ESM-2 embeddings, as to be expected. The performance and usefulness may be shown more clearly when tested in other computational biology problem settings.

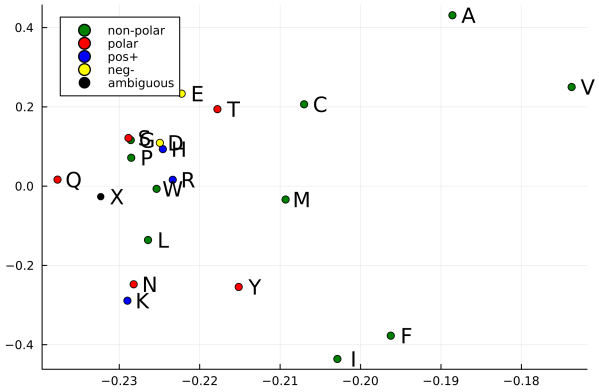

(a) Unaltered 1024-dimensional ESM-2 embeddings

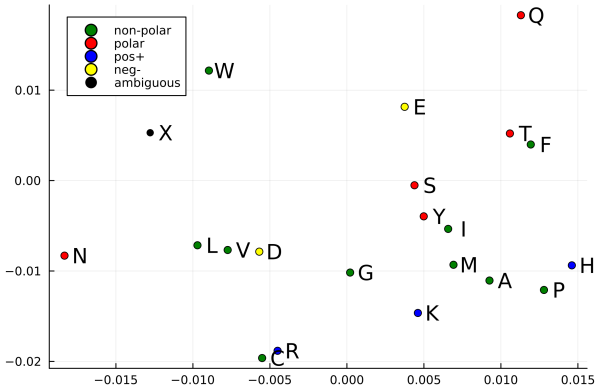

(b) ESM-2 embeddings projected into binary hyperdimensionality

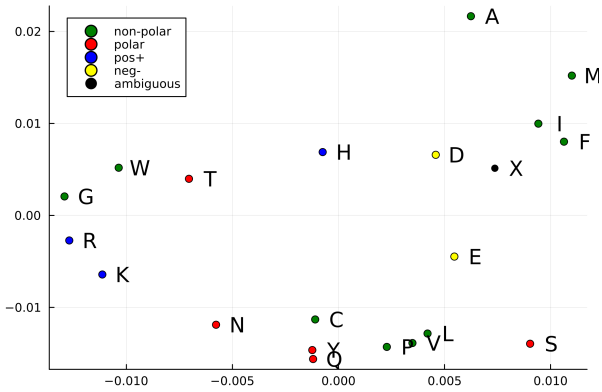

(c) Real-value projected ESM-2 embeddings.

Figure 3.4: Scatter-plots of the first two principal components of ESM-2 embeddings for amino acids. (a) Unaltered 1024-dimensional ESM-2 embeddings, accounting for roughly 79 % of the total variance. (b) ESM-2 embeddings projected into hyperdimensionality, accounting for roughly 22 % of the total variance. (c) real-valued projected ESM-2 embeddings, accounting for roughly 28.5 %. In all subfigures, amino acids are annotated and colored based on their chemical property of polarity.

3.5.2 Real-valued projected ESM-2 embeddings

The PCA of the real-valued projected ESM-2 vectors, as seen in figure 3.4c, appears to capture a greater proportion of the variance compared to their

binary counterparts. This increased detected variance is likely attributed to the reduction in data loss that occurs when avoiding the rounding off of values. The effectiveness of these real-valued projected ESM-2 vectors in various tasks will be further investigated and evaluated in subsequent analyses.

3.5.3 Enforcing similarities using genetic algorthims

The outcomes of employing a genetic algorithm to infer our target distances can be found in the tables located in Section A of the appendices. These are visually presented as heatmaps in figure 3.5. Taking into account that two random hyperdimensional vectors would be quasi-orthogonal just by stochastics, their Hamming distances would be close to 0.5. Hence, one could see that despite our efforts, our obtained distances remain significantly different from the desired values and still indicate quasi-orthogonality, which led us to discontinue further exploration of these vectors. This discrepancy is likely attributable to the vast search space associated with the problem, resulting in substantial computational time required to reach the target matrix. The optimization process ran for approximately 58 hours on a high-performance computing (HPC) system. Unfortunately, utilizing a genetic algorithm does not appear to be a viable method for optimizing hyperdimensional vectors within an acceptable timeframe.

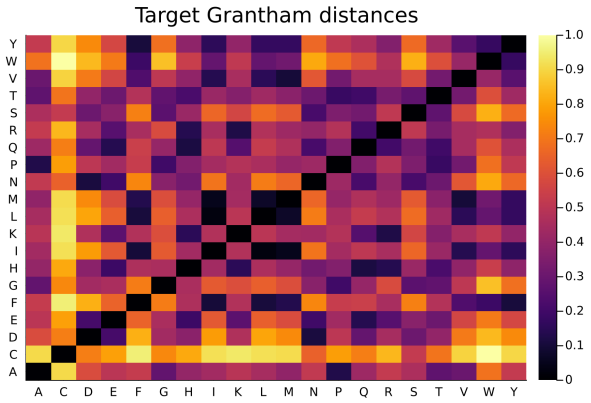

(a) Normalized Grantham's distance matrix.

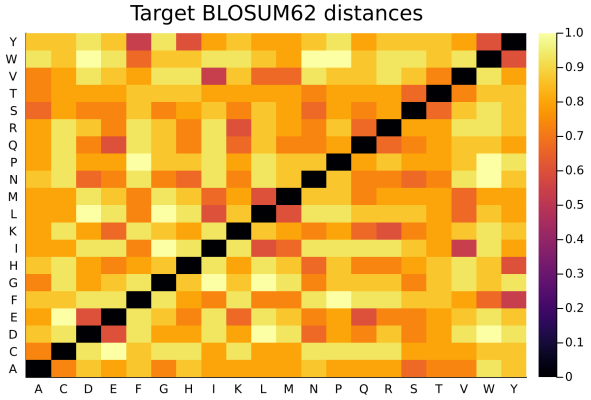

(b) Normalized amino acid distance matrix based on BLOSUM62.

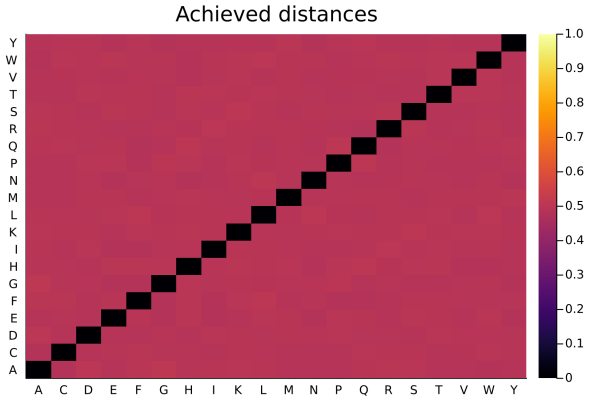

(c) Achieved similarity matrix.

Figure 3.5: Heatmap of the target pairwise amino acid distances, based on (a) Grantham's distance matrix (b) BLOSUM62 matrix and heatmap of (c) the achieved distances.

3.5.4 Contextualized neighborhood-encoding of amino acids

Looking at the average neighborhood-encoded amino acids starting from ESM-2 embeddings and the human proteome (figures 3.6a and 3.6b), the charged amino acids seem to be grouped vertically by PC 2, roughly dividing

the polar and non-polar amino acids, albeit slightly more pronounced for $n = 50$. Also interesting, to see very similar groupings in the PCA plots might indicate that the first four amino acids before and after a residue are the most crucial.

The PCA scatter plots generated from random vectors (figures 3.6c and 3.6d) show slightly different results as compared to the ones starting from ESM embeddings. These PCAs also capture less variance, which may indicate that encoding biological information/similarities into the vectors beforehand might be useful. For $k = 4$, some typicalities are noticed such as the close grouping of the negatively charged amino acids (D and E) and the consistent triangular grouping of H, L and R. Nonetheless, for $k = 50$ with random vectors, we see results deviating from all the PCA scatter plots of other neighborhood-encoded amino acids, which could mean that a PCA is not able to capture the sparse information for this case or that these vectors might be oversaturated.

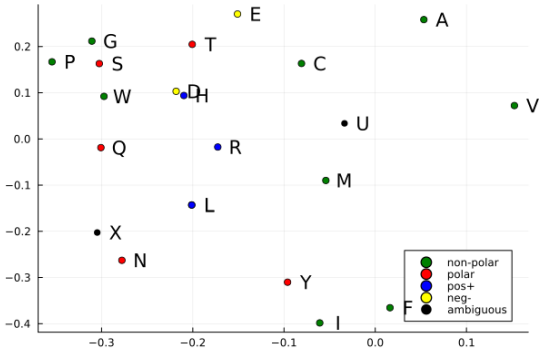

(a) $n = 4$ from projected ESM-2 embeddings, accounting for 21 % of the total variance.

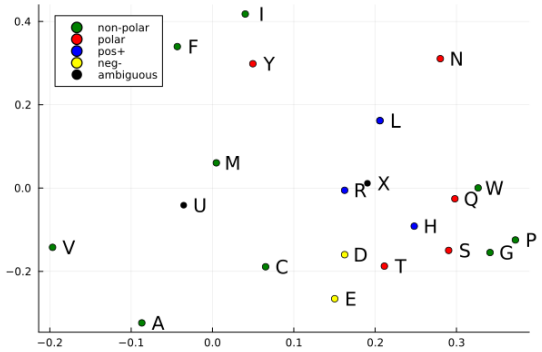

(b) $n = 50$ from projected ESM-2 embeddings, accounting for 21 % of the total variance.

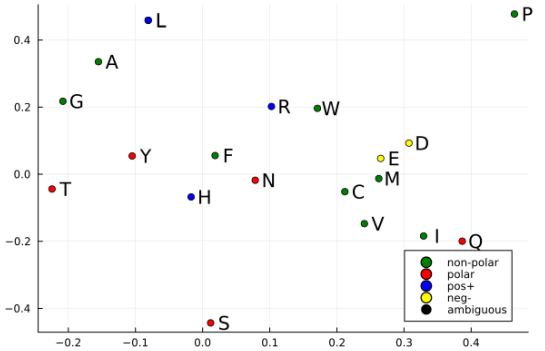

(c) $n = 4$ from random vectors, accounting for 11 % of the total variance.

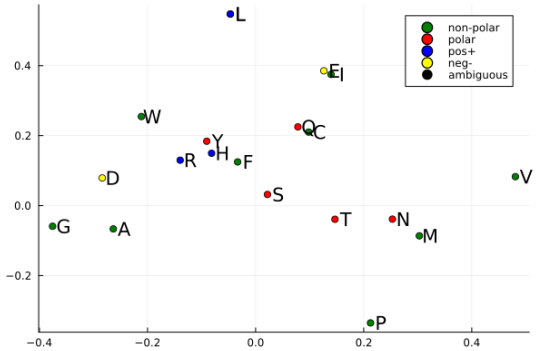

(d) $n = 50$ from random vectors, accounting for 11 % of the total variance.

Figure 3.6: Scatter-plots of the first two principal components of the average amino acid HDVs with neighborhood-information of $n = 4$ and $n = 50$ encoded, learned from the human reference proteome. The top row represents encoded amino acids starting from projected ESM-2 embeddings, and the bottom row represents encoded amino acids starting from random hyperdimensional vectors. The amino acids are annotated and colored based on their chemical property of polarity.

3.6 Discussion

As our research into genetic algorithms was unsuccessful for hyperdimensional vectors, future research could focus on other types of optimization algorithms such as simulated annealing [] etc. to generate optimized sets of hyperdimensional vectors in acceptable timeframes.

In Rives *et al.* (2011), they conducted experiments using their transformer model, ESM-1b [44], paralleled our attempts at projecting the neighborhood-encoded vectors into fewer dimensions. Our results are comparable to theirs, but not as cleanly grouped, which is likely due to several factors. For instance, due to the intrinsic stochastic nature of hyperdimensional computing, it is prone to capture some amount of noise. On top of this, it is difficult for dimensionality-reduction methods such as PCA to accurately capture the

intricacies of 10,000-dimensional vectors into 2 dimensions. UMAP projections were also made for the resulting vectors of the neighborhood-encoder method, shown in appendix A, but these did not reveal any new information. Future work could focus on refining projection methods for hyperdimensional vectors or exploring alternative data reduction techniques that are able to accurately visualize hyperdimensional data.

For specifically the neighborhood-encoder method, the amount of data we used is not comparable to what Rives *et al.* used in their training model: our method learned from fewer than 21,000 sequences whilst their model was trained on 250 million sequences. They also included sequences originating from all recorded organisms in the UniProt database at that time whilst we confined ourselves to human sequences. Secondly, hyperdimensional vectors have a limited capacity, meaning long-range dependencies of a residue will saturate the hyperdimensional vector depending on the range. We can predict the angle between a bundled vector and a randomly selected vector from said bundle vector by $\Theta = \arccos(\binom{2k}{k}/2^{2k})$ with $2k+1$ equal to the number of sequences in the class [71]. This approximation is valid for bipolar/binary vectors in hyperdimensions $(\geq 10,000)$. This equation also suggests that an increase in dimensions will not influence the angle, so a 1,000,000-dimensional vector would not have more capacity than a 10,000-dimensional one. Evaluating this equation by considering random 1001 vectors in a bundled vector, so $k = 500$, results in an angle of $88.6°$. This indicates that a vector has a limited capacity: the more vectors we bundle together, the closer the angle will be to 90° and thus the more dissimilar the bundled vector becomes to its components. This results in the bundled vectors not being representative anymore of a given dataset. However, note that this equation assumes that the bundled vector is a bundle of purely random vectors, which is not the case for most of our embeddings; it only provides us with a rough idea about the bundling capacity of a hyperdimensional vector. As we would bundle amino acids or protein sequences with varying similarities, the bundling capacity could be different, warranting further research in this domain.

In the forthcoming two chapters, we will delve into practical case studies that draw upon the methodologies explored in this chapter, engaging with protein sequence datasets and executing predictive tasks therein. Chapter 4 is focussed on exploring classification tasks employing protein sequence embeddings, wherein we will research the power of hyperdimensional computing, on its own or in combination with established machine learning

methods. In Chapter 5, we shift our focus toward the classification tasks on amino acid vectors by using our neighborhood-encoder method to create contextualized embeddings of amino acids and neural networks to classify these.

4. PHALP CASE STUDY: HYPERDIMENSIONAL PROTEIN SEQUENCE EMBEDDING AND BINARY PROTEIN-LEVEL CLASSIFICATION

4.1 PhaLP database

To implement and evaluate hyperdimensional computing in typical problem settings in computational biology, the potential of hyperdimensional computing will be evaluated on the PhaLP dataset [1] in this chapter. PhaLP is a comprehensive database currently comprising more than 17,000 entries of phage lytic proteins, including much of their information such as their type, domains and tertiary structures. Phage lytic proteins are used by bacteriophages to infect bacterial cells. To cross the bacterial cell walls, phages use two different types of phage lytic proteins: virion-associated lysins (VALs) and endolysins. Phage lytic proteins also comprise one or more functional domains categorized into two classes: enzymatically active domains (EADs) and cell wall binding domains (CBDs) [72].

The escalating global antibiotic resistance crisis has necessitated the development of alternative strategies to combat bacterial infections [73]. One such promising alternative is enzybiotics, a class of enzyme-based antibiotics derived from phage lytic proteins. Phage lytic proteins are produced by bacteriophages during their lytic replication cycle and are responsible for breaking down the bacterial cell wall. As these proteins exhibit a high level of diversity, it is critical to make well-informed selections during the early stages of research and development. In response to this need, Criel *et al.* introduced PhaLP [1], a comprehensive, automatically updated, and easily accessible database containing more than 17,000 phage lytic proteins.

PhaLP aims to serve as a portal for researchers, allowing them to access all relevant information about the current diversity of phage lytic proteins through user-friendly search engines. This database is specifically designed to facilitate the development and application of enzybiotics by providing a wealth of data on protein architecture, evolution, and bacterial hosts corresponding to the phages. PhaLP not only serves as a valuable starting point for the broad community of enzybiotic researchers but also offers continually improving evolutionary insights that can act as a natural inspiration for protein engineers. By enabling researchers to make well-considered selections of phage lytic proteins during the early stages of their projects, PhaLP plays a significant role in the development of highly effective, narrow-spectrum antibiotics. These enzybiotics have the potential to revolutionize the field of antibacterial agents, offering a much-needed response to the alarming threat of antibiotic resistance that plagues healthcare systems worldwide.

To fully utilize the rich content of PhaLP, the researchers conducted a series of analyses at three levels to gain insights into the host-specific evolution of phage lytic proteins. First, they provided an overview of the modular diversity of these proteins. This was followed by the adoption of data mining and interpretable machine learning approaches to reveal host-specific design rules for domain architectures in endolysins. Lastly, the evolution of phage lytic proteins at the protein sequence level was explored, uncovering host-specific clusters.

In this chapter, we will explore the authors' experiment on protein classification based on sequence data and evaluate the potential of hyperdimensional computing in the context of protein functional annotation. The primary objective is to better understand the role of hyperdimensional computing in protein classification and to elucidate its potential advantages over conventional machine learning techniques.

4.2 Type classifcation

The developers of PhaLP aimed to classify protein sequences based on their type, with a focus on two types of phage lytic proteins: virion-associated lysins (VALs) and endolysins. Both of these proteins play crucial roles in the lytic replication cycle of bacteriophages, as they help the viruses breach the bacterial cell wall. VALs are an integral component of the viral particle,

and their primary function is to create a small pore in the peptidoglycan layers of the bacterial cell wall at the infection site. This process allows the bacteriophage to gain access to the interior of the bacterial cell, initiating the lytic replication cycle. On the other hand, endolysins are produced within the infected bacterial cell and act toward the end of the replication cycle. These enzymes degrade the peptidoglycan layer of the bacterial cell wall, leading to cell lysis and the release of new viral particles [1].

Only a fraction of the database is manually annotated to include the protein's type because the amount of phage lytic proteins whose type is described in the literature is relatively small. The developers of PhaLP resorted to a machine learning approach for the classification of unannotated sequences. The authors embedded each protein sequence *via* SeqVec [74] and trained a random forest classifier [75] with 100 estimators and balanced weights to classify the proteins whose types were unknown. For this case study, we attempted to simulate their experiments of classifying the proteins into the two types based on their sequence using several techniques based on hyperdimensional computing.

4.3 Methods

As of March 2023, the latest version of the PhaLP database, *v2021_04*, has been used to test our models. This dataset consists of 17,356 unique amino acid sequences of phage-lytic proteins.

Embedding of sequences into hyperdimensional vectors

First, we used the two sequence encoding techniques as discussed in section 3.4.2 to embed the protein sequences in hyperdimensional space. These methods have been applied to all sequences in the dataset that were manually annotated on their type using both random hyperdimensional vectors and projected ESM-2 embeddings. These were then visually assessed *via* PCA. To confirm the diversity of sequences within the types, pairwise global alignments of every possible non-ambiguous combination of sequences within the two types were performed using the BioAlignments.jl package with a BLOSUM62 scoring matrix and -5 penalty for gaps. All scores within a type are then averaged out.

Classification of hyperdimensional protein sequence embeddings

To discriminate, we experimented with 3 different methods: the rudimentary hyperdimensional computing classification as seen in section 2.3, an XGBoost classifier and by A. Hernandez-Cano *et al.* [76]. As in the PhaLP study, we use all non-ML annotated proteins in the dataset. Out of the 11549 unambiguous UniParc accessions in the newest version of the database, 4829 are manually annotated on their type. Out of these manually annotated proteins, 2803 are endolysins and 2026 are VALs. For all classification tests, the F1-score is used as a performance metric as we want to measure the overall performance of the methods. The F1-score is the harmonic mean of the precision and recall and could be interpreted as a weighted accuracy. This accounts for the slight unbalance in the dataset. All methods were evaluated *via* a stratified 10-fold cross validation.

Naive additive method

As a baseline level, we use the rudimentary HDC classification technique as seen in section 2.3: the binary HDVs of sequences of the same class are bundled to construct single HDVs representative of every class. Then, a sequence's class is inferred by comparing the sequence's HDV to both class HDV *via* a similarity measure based on the assumption that the class vector is maximally similar to its components.

XGBoost classifier

The baseline hyperdimensional classification method has been compared to a more established method, the XGBoost classifier [77]. The classification with an XGBoost classifier is done via the default XGBoost classifier from *XGBoost.jl v2.2.5* using the binary hyperdimensional embeddings as an input.

OnlineHD methods

Another method we experimented with, is OnlineHD by A. Hernandez-Cano *et al.* [76]. It is an algorithm that expands on the classical hyperdimen-

sional training methods by trying to eliminate model saturation. Instead of naively bundling vectors on top of each other, this algorithm assigns weights to every addition depending on how much new information it adds to the model to prevent class vector saturation. To train the model, assume a new data point V with label l and class vectors C_i with each having a label i. The cosine similarity of V with every class vector is then calculated (denoted as $cos(V, C_i)$ with i being a label). If V with an actual label l would have been predicted as l', the class vectors will be updated as followed (with learning rate η as a tunable hyperparameter):

$$C_l \leftarrow C_l + \eta(1 - cos(V, C_l)) * V \tag{4.1}$$

$$C_{l'} \leftarrow C_{l'} - \eta(1 - cos(V, C_{l'})) * V \tag{4.2}$$

This means that if a new data point is highly dissimilar to its class vector and thus contains a high amount of new information, the weight of the update ($\eta(1 - cos(V, C_i))$) will be high. The information is then also subtracted from the incorrectly predicted class vector. If a label would be correctly predicted for a new data point, the model will not be updated to avoid saturation. To initialize the model, the first vector of a class to be assessed is assumed to be the class vector. For example, if a query vector in our dataset is predicted to be a VAL, but its actual label is endolysin, the class vectors are then updated as followed:

$$C_{VAL} \leftarrow C_{VAL} + \eta(1 - cos(V, C_{VAL})) * V \tag{4.3}$$

$$C_{endo} \leftarrow C_{endo} - \eta(1 - cos(V, C_{endo})) * V \tag{4.4}$$

Due to the nature of this model, we cannot constrict our hyperdimensional embeddings to a bipolar or binary nature anymore and the embeddings are thus allowed to be real-numbered. Mathematical operations such as multiplications and additions are then assumed to be element-wise. On top of the single-pass method as discussed above, A. Hernandez-Cano *et al.* also implemented an iterative retraining algorithm to increase the accuracy of OnlineHD. This starts from the class vectors made *via* the single-pass OnlineHD model, but assesses the class vectors by performing inference with every training vector. If a training vector's label is wrongly predicted, equa-

tions 4.1 and 4.2 are then used to update the model. This entire sequence is iterated over a given amount of cycles.

Since these algorithms are only available as PyTorch implementations, implementations in Julia have been made here. A stratified 10-fold cross validation of these models with our subject sequences has been performed. The learning rate is set at 0.035 for both the single-pass and the iterative method and the amount of retraining iterations for the iterative method is set to 120 as these are the values set by default in their PyTorch package. To test these algorithms, real-numbered embeddings had to be made from our subject sequences. So instead of embedding the sequences starting with random bitvectors, random vectors with values in interval $[-1, 1]$ for both the random amino acid vectors and projected ESM-2 embeddings were made to obtain real-valued hyperdimensional vectors for every amino acid. The same bag-of-words and convolutional approaches as discussed in Section 3.4.2 have been applied here to obtain real-valued sequence embeddings. These were assessed *via* a scatter-plot of the two first principal components of their PCA projection.

To monitor the training procedure of an OnlineHD single-pass model, the same procedures as above are followed, but without the cross validation. The absolute difference between the cosine similarities, $cos(V, C_{VAL})$ and $cos(V, C_{VAL})$ as described in equations 4.3 and 4.4, has then been calculated for each query vector before the update. The results are shown in Figure 4.3 for every combination of amino acid- and sequence embedding methods. Another approach to monitor the training procedure is to track the two class vectors C_{VAL} and C_{endo} individually. For each query vector V_l with a known label l, we calculate the cosine similarity $cos(V_l, C_l)$. The results are shown in Figure 4.4 for every combination of amino acid- and sequence embedding methods.

To follow the training procedure in terms of performance, the dataset is divided into training and testing sets, while ensuring stratification is preserved, with the test set comprising 10 % of the data. The training data is further partitioned into 500 batches, and the model is trained incrementally using these batches. After each batch has been processed, the model's performance on the test data is assessed to provide insights into its learning trajectory with the results shown in Figure 4.5 for every combination of amino acid- and sequence embedding methods.

4.4 Results

Embedding of sequences into hyperdimensional vectors

There is no visual difference between the PCA plots for the sequences embedded *via* the bag-of-words method and the convolutional method, but there is a clear difference between the different starting embeddings as seen in Figure 4.1. The binary sequence embeddings from both the bag-of-words method and the convolutional method made with ESM-2 AA embeddings seem to capture more of the variance between the sequences.

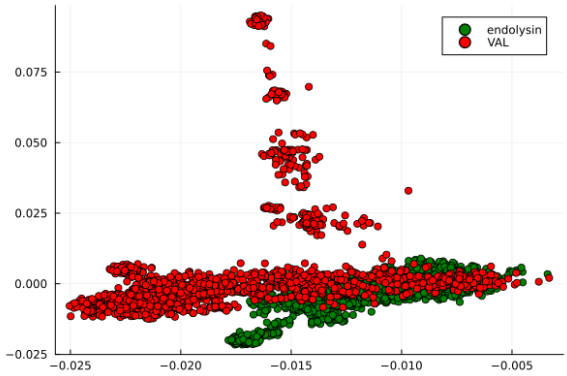

(a) BoW-encoded protein sequences, starting from random vectors. These PCs account for roughly 7 % of the total variance in the system.

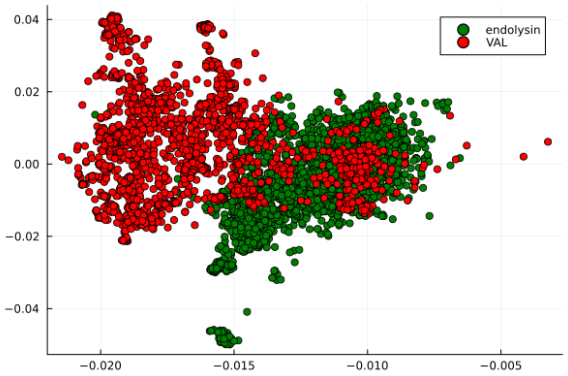

(b) BoW-encoded protein sequences, starting from projected ESM-2 embeddings. These PCs account for roughly 15.5 % of the total variance in the system.

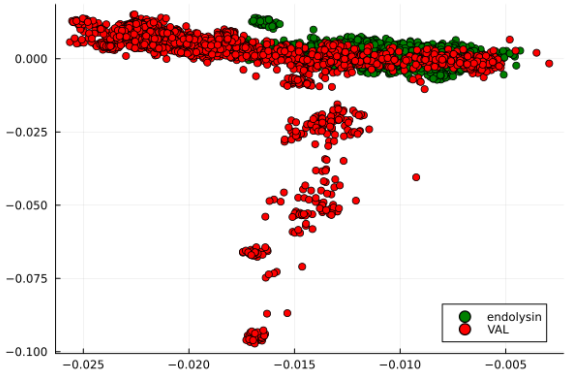

(c) Convolutionally encoded protein sequences, starting from random vectors. These PCs account for roughly 7 % of the total variance in the system.

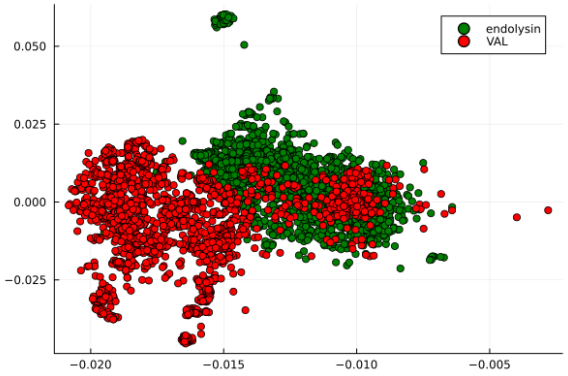

(d) Convolutionally encoded protein sequences, starting from random vectors. These PCs account for roughly 15.5 % of the total variance in the system.

Figure 4.1: Scatter-plot of the first two principal components of the binary encoded phage lytic proteins *via* the BoW-method starting from (a) random HDVs per amino acid (b) projected ESM-2 amino acid embeddings and *via* the convolutional method from (c) random HDVs per amino acid (d) projected ESM-2 amino acid embeddings. Only manually annotated phage lytic proteins were considered and are color-coded based on their type.

As with the binary embeddings, PCA of the real-valued sequence embeddings shows no distinction between those made *via* the bag-of-words

method and the convolutional method whilst showing a clear difference between the different starting embeddings as seen in Figure 4.3. Similarly, the explained variance is much higher for embeddings made with projected ESM-2 embeddings. However, the PCA method retrieves much more information from real-valued embeddings. From all the PCA scatter plots mentioned, we can estimate by the sparser distribution of the VAL proteins that these would be slightly more diverse in sequence than endolysins.

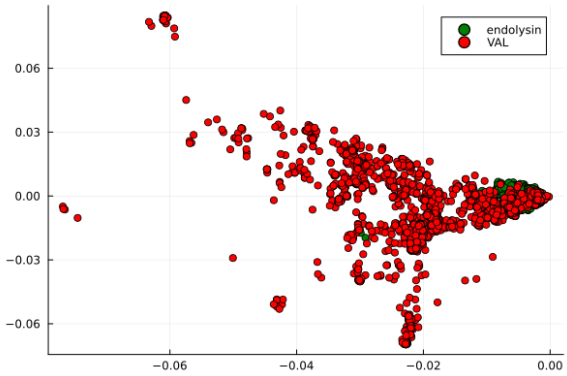

(a) BoW-encoded protein sequences, starting from random vectors. These PCs account for roughly 30.4 % of the total variance in the system.

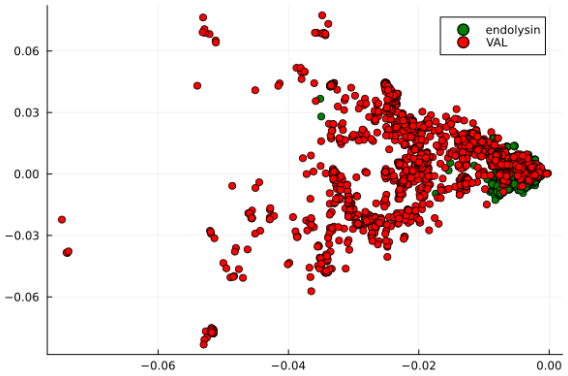

(b) BoW-encoded protein sequences, starting from projected ESM-2 embeddings. These PCs account for roughly 57.3 % of the total variance in the system.

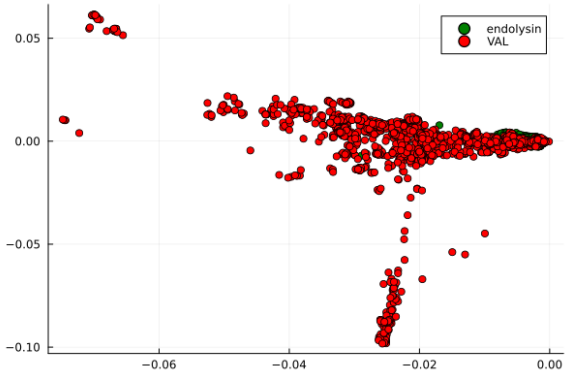

(c) Convolutionally encoded protein sequences, starting from random vectors. These PCs account for roughly 30.4 % of the total variance in the system.

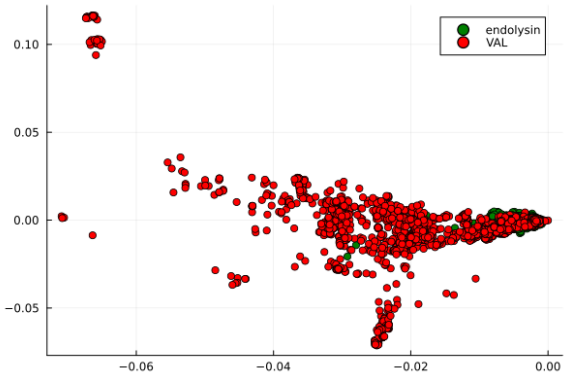

(d) Convolutionally encoded protein sequences, starting from projected ESM-2 embeddings. These PCs account for roughly 57.3 % of the total variance in the system.

Figure 4.2: Scatter-plot of the first two principal components of the real-valued encoded phage lytic proteins *via* the BoW-method starting from (a) random HDVs per amino acid (b) projected ESM-2 amino embeddings and *via* the convolutional method from (c) random HDVs per amino acid (d) projected ESM-2 amino embeddings. Only manually annotated phage lytic proteins were considered and are color-coded based on their type.

In each of the PCA projections previously discussed, VALs consistently exhibited a higher degree of diversity in comparison to endolysins. To validate this observation, pairwise alignments were conducted across all sequences within their respective groups. VAL proteins yielded an average score of -209, while the endolysins scored -7. This pronounced disparity in scores shows greater intra-group dissimilarity among the VAL sequences as op-

posed to those of the endolysins, confirming our findings in the PCA projections.

Classification of hyperdimensional protein sequence embeddings

The resulting F1-scores from our 4 classification methods are listed in Table 4.1. Evaluating our naive additive model using stratified 10-fold cross-validation results in F1-scores of around 0.14 for every kind of amino acid embedding.

Table 4.1: Results of type classifications using the principal classification technique of hyperdimensional computing, an XGBoost classifier and OnlineHD implementations with several kinds of embeddings. Note that the OnlineHD-based models were developed using real-valued embeddings.

F1-scores	**BoW/random**	**BoW/ESM**	**Convolutional/random**	**Convolutional/ESM**
Naive addition	0.1458	0.1468	0.1461	0.1461
XGBoost classifier	0.9667	0.9754	0.9661	0.986
Single-pass OnlineHD	0.8901	0.9214	0.7793	0.8400
Iterative OnlineHD	0.9487	0.9757	0.9486	0.9670

The scores of the XGBoost classifier with our sequence embeddings are much more comparable to the results of the experiment in the PhaLP paper, with the convolutional embeddings generally performing better than the bag-of-words embeddings and also the ESM 2-based performing better than random base vectors when considering the type of amino acid vectors used. This is an indication that hyperdimensional computing can provide a very fast and reliable method of embedding protein sequences, even without prior biological information. The drawback of this machine learning model, which is to be expected from every gradient-based model, is that training and predictions take much longer to compute compared to hyperdimensional training models. The cross validation procedure took up to 5 minutes on a consumer-grade laptop, whilst with the naive additive approach, the procedure took less than 10 seconds to finish.

Comparing the results of the OnlineHD models to the naive additive HDC model, we can see a substantial increase in the performance of this model. The single-pass model seems to have more widely varying results depending on the type of embeddings used. As opposed to the XGBoost classifier, it performs better using bag-of-words embeddings. The model also performs better when trained with embeddings based on projected ESM-2 vectors.

Iterative retraining of the model seems to increase its performance significantly, even coming close to the performance of an XGBoost classifier in this case. Further improvement might be found when optimizing the models' parameters. The cross validation procedure takes less than 10 seconds to run for the single-pass model, whilst doing an iterative retraining of the model adds 2 to 3 minutes. This model appears to be a decently performing extension of the rudimentary hyperdimensional classification model for protein classification, whilst still being much more efficient than the commonly used machine learning models. The drawback of the model is that we cannot use hyperefficient bit-operations anymore, which limits its efficiency compared to the binary nature of the additive model.

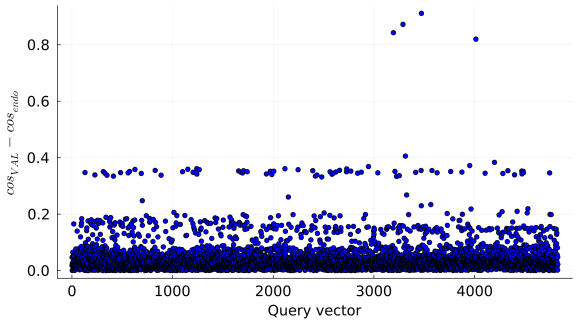

(a) Embeddings using random amino acid vectors, made *via* the bag-of-words embedding method

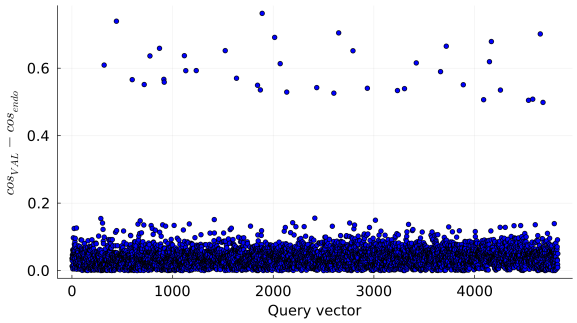

(b) Embeddings using projected ESM-2 amino acid vectors, made *via* the bag-of-words embedding method

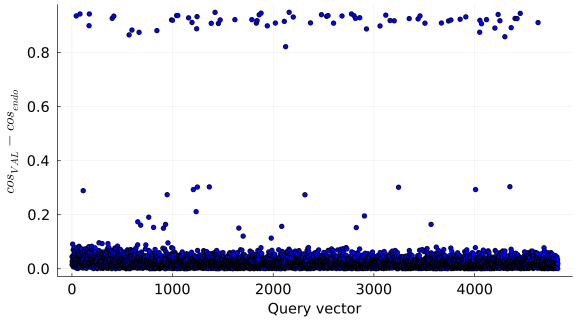

(c) Embeddings using random amino acid vectors, made *via* the convolutional embedding method

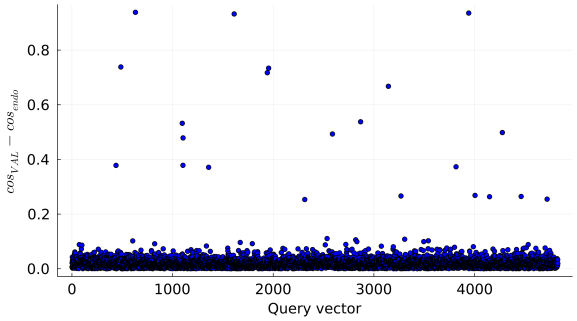

(d) Embeddings using projected ESM-2 acid vectors, made *via* the convolutional embedding method

Figure 4.3: Absolute difference between the cosine similarity of the query vector with the VAL class vector and the cosine similarity of the query vector with the endolysin class vector before the weighted update while following the OnlineHD single-pass training procedure. Trained using hyperdimensional embeddings from all protein sequences in the PhaLP dataset whose types were manually annotated.

To further research the power of OnlineHD, we aim to monitor its training procedure when applied to the PhaLP dataset. We calculate the absolute difference between the cosine similarities, $cos(V, C_{VAL})$ and $cos(V, C_{endo})$, as described in equations 4.3 and 4.4. By observing this metric, we can gain insights into the behavior of the hyperdimensional vectors in the OnlineHD model during training. A possibility to expect is that the difference in cosine similarities increases throughout the training procedure as the model learns

to differentiate the two classes. However, these differences don't increase noticeably in this case as shown in Figure 4.3.

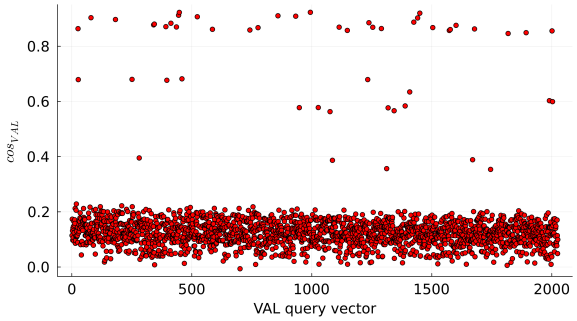

(a) VALs embedded using random amino acid vectors *via* the bag-of-words method

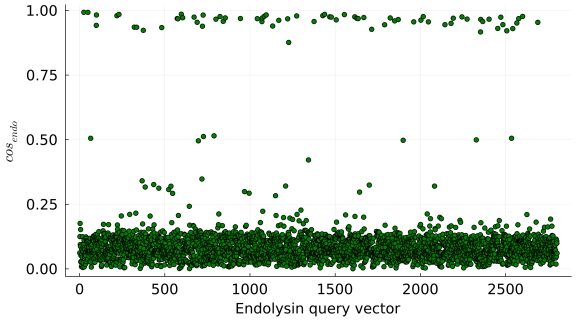

(b) Endolysins embedded using random amino acid vectors *via* the bag-of-words embedding method

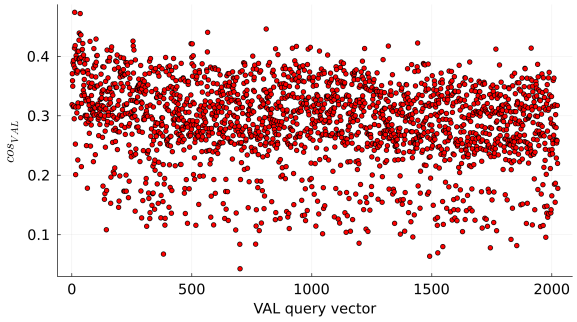

(c) VALs embedded using projected ESM-2 amino acid vectors *via* the bag-of-words embedding method

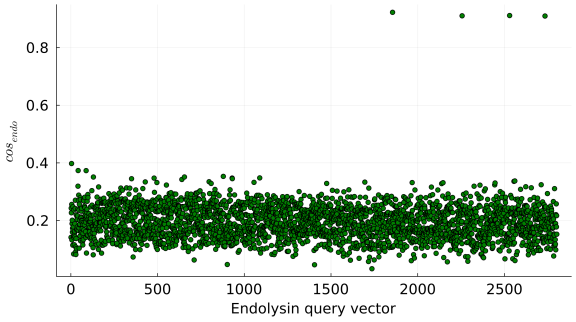

(d) Endolysins embedded using projected ESM-2 amino acid vectors *via* the bag-of-words embedding method

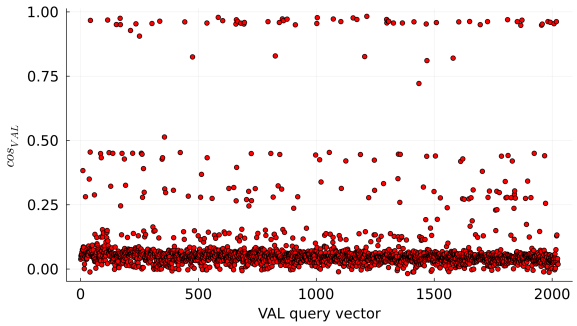

(e) VALs embedded using using random amino acid vectors *via* the convolutional embedding method

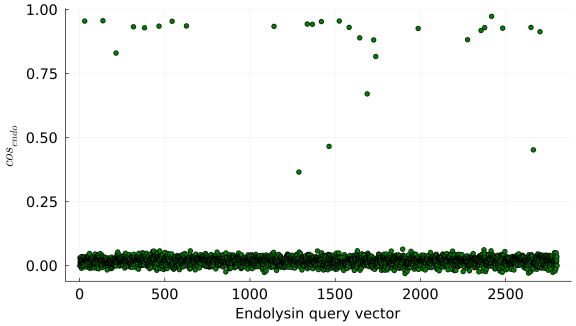

(f) Endolysins embedded using random amino acid vectors *via* the convolutional embedding method

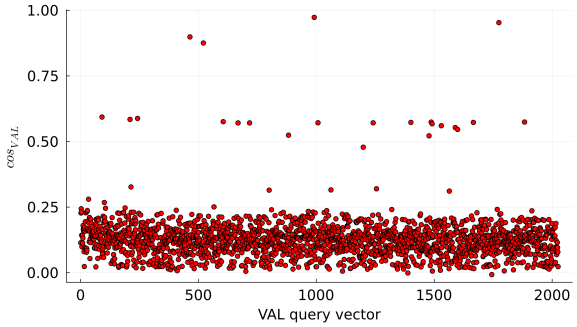

(g) VALs embedded using projected ESM-2 amino acid vectors *via* the convolutional embedding method

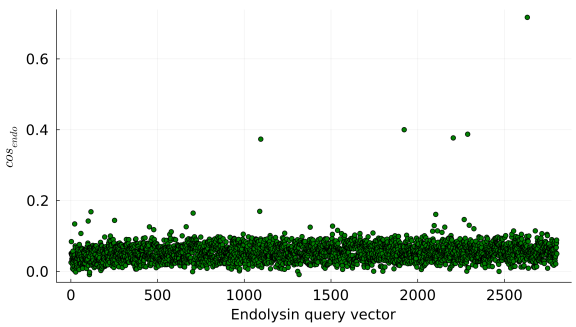

(h) Endolysins embedded using projected ESM-2 amino acid vectors *via* the convolutional embedding method

Figure 4.4: Cosine similarity between a query vector and the class vector before the weighted update during OnlineHD single-pass training procedure. Trained using hyperdimensional embeddings from all protein sequences in the PhaLP dataset whose types were manually annotated, red representing VALs and green representing endolysins.

Another approach to monitor the training procedure is to track the two class vectors C_{VAL} and C_{endo} individually. For each query vector with a known label l, we calculate the cosine similarity $cos(V_l, C_l)$. This method allows us to observe the model's adaptation and refinement of its internal representation of the two classes before it predicts a query vector during the training process. The distance between a query vector and a class vector is proportional to the update weight, so we expect the cosine similarities to generally increase as the model learns. The results are shown in Figure 4.4.

In this case, the VAL vector shows near-consistent weight updates, indicating a high likelihood of the dataset being diverse as the cosine similarities don't seem to decrease. This consistent learning pattern also suggests that the method effectively extracts and learns from the diverse information embedded in the dataset. In general, we see a higher variation in cosine similarities for VAL vectors, which suggests that virion-associated lysins are more diverse in sequence compared to endolysins. This also confirms our earlier findings. We also notice higher overall similarities between the query vectors and the VAL vector when using the BoW-method with projected ESM-2 vectors compared to other embedding methods, which aligns with this model's superior performance. The endolysin vector appears to be updated at a constant rate too, with less variation in similarities. As observed with the VAL vectors, the similarities between the query vectors and the endolysin vector are higher when the embeddings are created using the BoW-method with projected ESM-2 vectors.

Instead of looking at the inner workings of the OnlineHD method, the training progress of an OnlineHD model in terms of performance has been monitored. This progress is visualized in Figure 4.5. Upon initial observation, it is apparent that the models trained with embeddings generated using the convolutional method exhibit superior performance from the outset. This higher starting point might be partially attributed to the random initialization of the model. However, a common characteristic observed across all models is that their performance tends to stagnate after roughly 100 batches, which corresponds to roughly 870 sequences in our case. This observation suggests that hyperdimensional computing-based classification methods may exhibit promising performance and effectively capture essential information, even after being exposed to just a small fraction of the training data, which is an intriguing finding for further exploration.

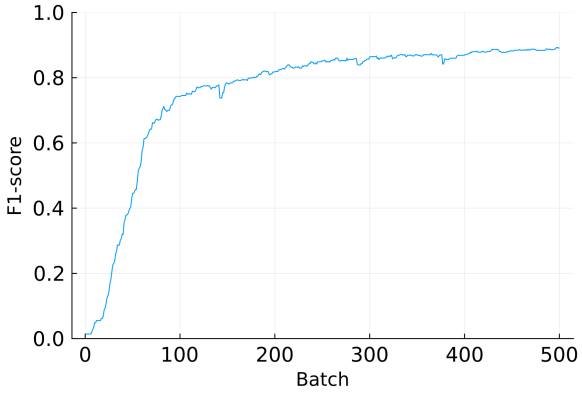

(a) Embeddings using random amino acid vectors, made *via* the bag-of-words embedding method

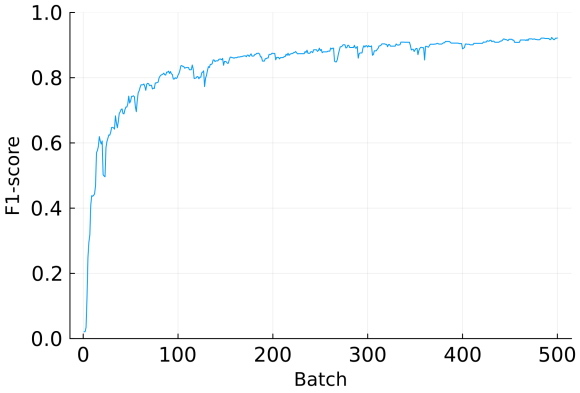

(b) Embeddings using projected ESM-2 amino acid vectors, made *via* the bag-of-words embedding method

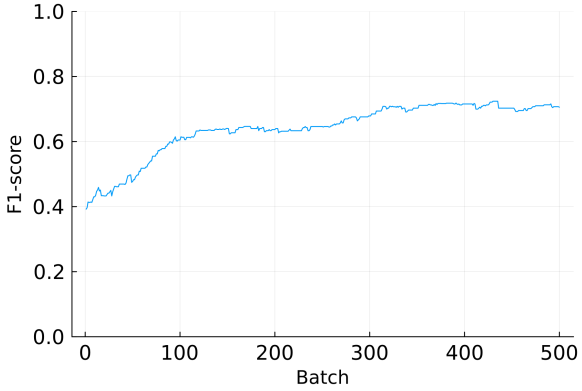

(c) Embeddings using random amino acid vectors, made *via* the convolutional embedding method

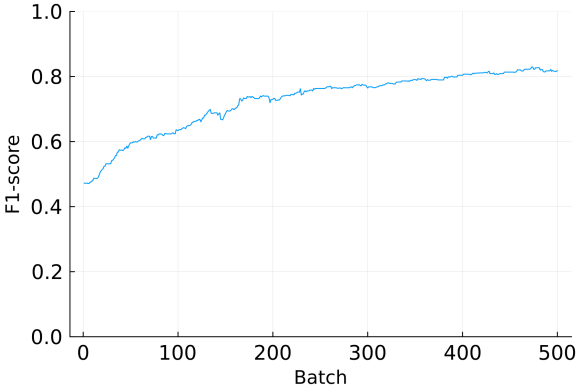

(d) Embeddings using projected ESM-2 acid vectors, made *via* the convolutional embedding method

Figure 4.5: The F1-score of the OnlineHD single-pass model with a validation set throughout its training procedure. Trained in batches using several kinds of hyperdimensional embeddings from all protein sequences in the PhaLP dataset whose types were manually annotated.

4.5 Discussion

The low scores of the naive additive methods are likely due to the possibility of oversaturation of the class vectors as discussed in section 3.6. Thus, using the rudimentary model works only for very small datasets, as seen in the examples in chapter 2.3. The ability of this method to learn from a small dataset can be very useful, but backfires in terms of performance when applied to large and diverse datasets as we have seen in the case of classifying protein sequences from the PhaLP database.

This issue is mitigated in the OnlineHD method when used in classifications as it applies weights to class vector updates. This results in a substantial increase in performance. When paired with an iterative retraining procedure its performance comes close to the performance of established machine learning methods paired with binary hyperdimensional sequence embed-

dings. The OnlineHD methods require real-valued vectors, but still show much higher computational efficiencies compared to established machine learning methods.

From the results in Figures 4.3 and 4.4, we could not conclude using similarities of query vectors to the class vectors as a metric for training monitoring, as these more likely represent the variety in the training data, especially visible in Figure 4.4 as the better-performing models show that they capture more of the intricacies of the input data.

Looking at OnlineHD's performance during its training procedure in Figure 4.5, we noticed that it is able to capture a lot of information with only a small set of the data, which warrants further study. To further investigate the potential of OnlineHD for protein-level classification in future research, we could investigate how it could classify the sequences based on other types of information present in the PhaLP database such as host type and domains.

Upon comparing various methods for amino acid encoding, we find that dimension-reduction methods tend to capture more information from sequence embeddings created with projected ESM-2 vectors. This observation is consistent with our other finding where we consistently noted an enhanced performance in our classification task using these amino acid vectors. However, our analysis was limited to a single dataset and one specific task; consequently, further investigation is essential. Future studies should focus on the development and evaluation of alternative tasks, while also testing the applicability of this method across various biological datasets.

As for the sequence embedding methods, while no visual differences were discernible after applying PCA to the protein sequences, the results varied subtly depending on the specific model used for classification. Therefore, it appears that there may not be a significant difference in how information is being captured between the two sequence embedding methods in our case. This may indicate that encoding positional information into the k-mers may not be necessary to capture information on protein sequences as the BoW-method captures enough essential information in our case. Nevertheless, future research should discern the potential utility of this in the context of other datasets and predictive tasks.

5. HYPERDIMENSIONAL COMPUTING METHODS FOR AMINO ACID-LEVEL PREDICTIONS

5.1 Introduction

As discussed in section 1.3, state-of-the-art protein language models primarily rely on transformer-based architectures to learn representations of protein sequences and amino acids in the context of other amino acids [40]. These models have demonstrated their effectiveness in various applications, such as protein function prediction and protein-protein interaction prediction, by capturing complex patterns in amino acid sequences [52]. Moreover, these models are also capable of making detailed predictions at the amino acid level, such as predicting secondary structure. This involves determining local conformations of regions within a protein, such as alpha-helices and beta-sheets, based on the sequence of amino acids. This capability further extends their utility in understanding protein structure and function. However, these models are computationally intensive and may be less suitable for certain tasks or scenarios where computational resources are limited.

In section 3.4.1, we explored the idea of encoding information from a residue's neighborhood into a hyperdimensional vector that represents the residue and its surroundings. This approach allows us to capture local sequence information and can serve as an effective encoding scheme for amino acids. To evaluate the effectiveness of this encoding method, we will employ it as an input for several perceptron-based models.

Perceptron-based models, a type of artificial neural network model, have been employed for various machine learning tasks over the years, including

classification and regression problems. The perceptron, one of the simplest and earliest types of neural networks, was proposed by Frank Rosenblatt in 1958 [78]. A perceptron consists of a single artificial neuron that receives multiple input features and computes a weighted sum of these inputs. This weighted sum is then passed through an activation function, which determines the output of the perceptron. The learning process involves adjusting the weights of the input features iteratively, using a rule that minimizes prediction errors on the training data. The perceptron learning algorithm starts with an initial set of weights, typically set to zero or small random values. For each instance in the training data, the perceptron computes the output, compares it with the true label, and updates the weights accordingly. The weight update rule is based on the difference between the predicted output and the true label, multiplied by the learning rate and the input feature value. Single-layer perceptrons consist of an input layer and an output layer of perceptrons, allowing for multiclass classifications. However, they can only solve linearly separable problems, limiting their applicability for more complex tasks.

As single-layer perceptrons can only solve linearly separable problems, researchers developed more complex neural network architectures, such as multi-layer perceptrons (MLP), which consist of multiple layers of artificial neurons connected in a feedforward manner. MLPs can learn non-linear patterns in the data by using non-linear activation functions (e.g., sigmoid, tanh, ReLU) and employing backpropagation for weight updates [79]. This enhanced ability to model non-linear relationships allows MLPs to tackle a wider range of problems.

By combining the residue neighborhood encoding method with perceptron-based models, we could develop more computationally efficient alternatives to state-of-the-art transformer-based models. These models may provide valuable insights into protein sequences and amino acids while being more suitable for scenarios with limited computational resources.

The aim of this chapter is to design and implement a simple perceptron-based neural network that utilizes hyperdimensional vectors of residues in a protein sequence as inputs. The goal is to train the network to discern and learn the secondary structure of these residues based on their surrounding counterparts. Ultimately, this should enable our model to accurately and efficiently predict the secondary structures of residues in protein sequences whose structure is unknown.

5.2 Methods

We built straightforward perceptron-based neural networks that take as input a hyperdimensional vector, in particular a neighborhood-encoded amino acid vector made as described in section 3.4.1. It should then output the amino acid's secondary structure, either 3- or 8-state as shown in Figure 5.1.

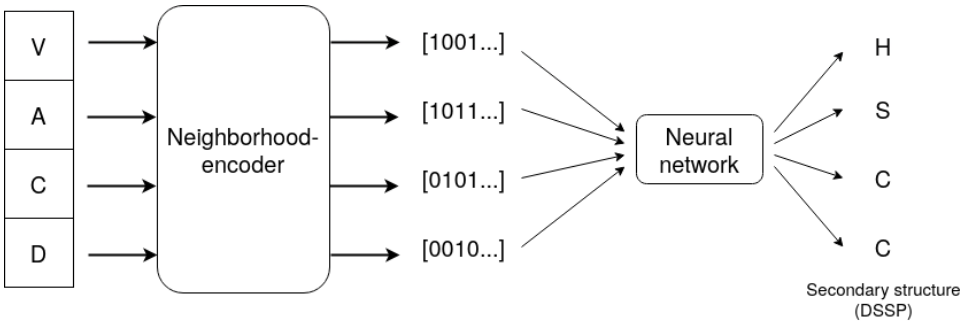

Figure 5.1: A simple demonstration of our pipeline to classify amino acids on their secondary structure based on their neighborhood-encoded vectors. First, a residue is encoded by neighborhood-encoding as discussed in section 3.4.1. Then, this vector is used as an input for a trained neural network to predict its secondary structure state. This is done for every residue in every given protein sequence.

We used the training dataset compiled by Klausen *et al.* for their model protein language model NetsurfP 2.0 [80] as our training dataset. It contains 10,337 protein sequences obtained from the Protein Data Bank (PDB) [35]. Each residue in these sequences is annotated with its 3- and 8-class secondary structure classification according to *Define Secondary Structure of Proteins* (DSSP) [81], providing a comprehensive description of the protein's structural properties. All residues have been encoded using our neighborhood-encoder as described in section 3.4.1 with $n = 25$ and $n = 100$ using random hyperdimensional vectors for each amino acid. Due to computational memory constraints, we randomly selected 60 % of the sequences from the original dataset for training and validation (80 % and 20 % respectively), ensuring a representative sample of the data.

In summary, we have four distinct supervised training sets. The first model is trained on neighborhood-encodings of range $n = 25$ with 3-state secondary structure labels. The second model also uses neighborhood-encodings of range $n = 25$, but with 8-state secondary structure labels. The third model is trained on neighborhood-encodings of range $n = 100$, using 3-state secondary structure labels. Finally, the fourth model uses

neighborhood-encodings of range $n = 100$ and 8-state secondary structure labels.

As for the perceptron-based methods, to decrease the computational time, we opted to build, train and evaluate the model in Python due to its support for computations on GPUs on our systems. We employed PyTorch Lightning v1.8.4 for model construction and training on a high-performance computing (HPC) cluster equipped with an NVIDIA V100 GPU. The model comprised fully-connected layers with an input layer size equal to the dimension of the hyperdimensional vectors (10,000 in this case). Depending on the secondary structure classification desired, the output layer size was set to either 3 or 8 depending on the secondary structure classification. We used a batch size of 128 during training. Between each layer, we incorporated a ReLU (Rectified Linear Unit) activation function to introduce non-linearity into the model. The training loss was monitored using cross-entropy loss. To optimize the model, we employed the widely-used ADAM optimizer. We evaluated various configurations and hyperparameters to determine the best-performing but still computationally feasible approach as shown in Table 5.1

Table 5.1: Overview of model configurations and hyperparameters tested

	Epochs	Learning rate	Size hidden layer(s)
SLP	100	0.03	/
1-layer MLP	50	0.003	500
10-layer MLP	200	0.0003	8000-5000-2000-1000-800-500-200-100-50-20

As test datasets, we opted to use CB513 [82] and CASP12 [83] (compiled by the developers of NetSurfP 2.0 [80]) since they are easily attainable and commonly used by researchers as benchmark datasets for protein language models. The MLP model with 10 hidden layers was trained and then evaluated using these test datasets. For extra validation, random data was generated in the form of random hyperdimensional vectors with randomly given labels.

5.3 Results

Figure 5.2 presents the outcome of the training procedure of all perceptron-based configurations with $n = 25$ and dssp3-classification. They show notable issues with the SLP models' ability to train effectively on our dataset.

This is signaled by the substantial fluctuations in both loss and validation performance, a trend suggesting an inherent instability in the learning process of this model. The SLP model also displayed a abnoramlly high error compared to the other configurations. The 1-layer MLP model also exhibits problematic behavior, as it does not seem to learn as seen in its constant loss-curve. On top of that, it predicts only one single class during validation (the class with the highest proportion), resulting in a large discrepancy between the accuracy and F1-score. All of this could be attributed to the simplicity of these models, which might not have the capacity to capture the complex patterns in the data. These limitations lead to our decision to discontinue further investigations and experimentation with these particular models. These behaviors were seen throughout all types of datasets (both *n*s and dssp-classifications) as seen in Figures B.1, B.2 and B.3 in the appendices.

In contrast to the SLP and the 1-layer MLP models, the performance of the much deeper 10-layer MLP model demonstrates much more stable and consistent behavior throughout the training process, as evidenced by the performance and loss metrics, even though the resulting performance remains generally low. Although this stability may partially result from the lower learning rate, the model's computational feasibility made it an option for further investigation, prompting us to select this 133,343,733-parameter model for our subsequent tests with various datasets and comparisons with other state-of-the-art methods.

Table 5.2: Accuracies of secondary structure classification of a 10-layer MLP model trained on 60 % of NetSurfP 2.0's training data encoded into different kinds of hyperdimensional embeddings made with neighborhood-encoding ($n = 25$ and $n = 100$). Tested on the CASP12 and CB513 dataset. Performance with randomly generated data was also assessed.

Accuracy	CASP12		CB513		Random	
	ss3	ss8	ss3	ss8	ss3	ss8
n25	36.9	24.88	35.48	21.01	34.11	21.09
n100	39.33	23.13	37.61	20.86	38.74	20.53

The fully trained 10-layer MLP models were evaluated on the test datasets with the results summarized in Table 5.2 and Table 5.3. To validate our findings, we also generated a randomly generated dataset for comparison. Disappointingly, the model's performance on the test data only slightly surpassed its own performance on the randomly generated data, meaning that our model is not able to accurately predict the secondary structure of an

Table 5.3: F1-scores of secondary structure classification of a 10-layer MLP model trained on 60 % of NetSurfP 2.0's training data encoded into different kinds of hyperdimensional embeddings made with neighborhood-encoding ($n = 25$ and $n = 100$). Tested on the CASP12 and CB513 dataset. Performance with randomly generated data was also assessed.

F1	CASP12		CB513		Random	
	ss3	ss8	ss3	ss8	ss3	ss8
n25	37.50	18.61	35.52	15.30	34.35	14.79
n100	37.19	20.25	35.68	18.03	36.07	17.80

Table 5.4: Accuracies of secondary structure classification of state-of-the-art protein language models. Tested on 3 and 8 secondary structure classifications of the CASP12 and CB513 dataset.

Accuracy	CASP12		CB513	
	ss3	ss8	ss3	ss8
ESM-1b	76.9	83.9	66.0	70.2
NetSurfP 2.0	82.0	84.5	66.9	71.3
NetSurfP 3.0	79.1	84.5	66.9	71.1
ProtT5-XL-U50	77.5	86.2	70.5	74.5

amino acid based on its neighborhood-encoding as compared to state-of-the-art protein language models shown in Table 5.4.

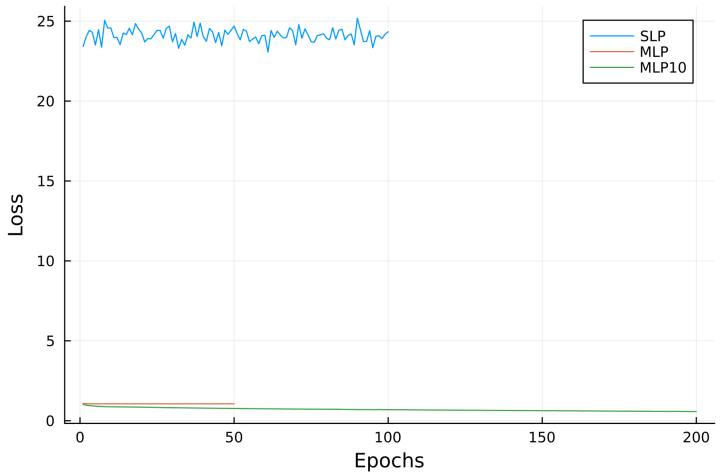

(a) Training losses

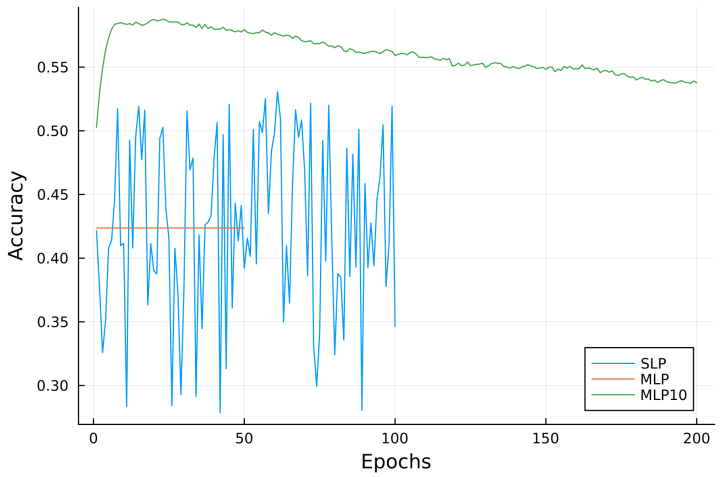

(b) Accuracies

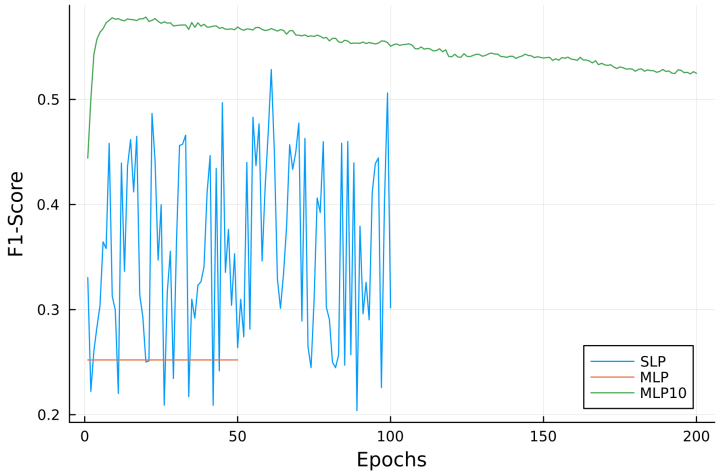

(c) F1-scores

Figure 5.2: (a) cross-entropy losses (b) accuracies (c) F1-scores of all perceptron-based configurations tested. Trained with neighborhood-encodings of 60 % of the training dataset of NetSurfP 2.0. Here $n = 25$ and the secondary structure classification is dssp3-based. Note that the SLP and 1-layer MLP model was evaluated using fewer epochs than their 10-layer counterpart.

5.4 Discussion

Our exploration into the use of various perceptron-based neural network models for protein secondary structure prediction has yielded several insights. The overarching observation from our results is that our models have not effectively learned from the data. This suggests a couple of potential areas for improvement.

Firstly, the relative simplicity of our neural network models may be a limiting factor. The high-dimensional sparse vectors that represent our data may require a more complex model to capture the intricate patterns within the data effectively. This could involve exploring more sophisticated architectures, such as deeper networks or alternative architectures. A hyperdimensional computing-based method such as OnlineHD might be an interesting learning method too for later research.

Secondly, the neighborhood-encoding algorithm we employed may require further refinement. The quality of the embeddings produced by this algorithm directly impacts the ability of the model to learn. Optimizing this algorithm to produce more informative or discriminative embeddings could potentially enhance the learning capability of our models. As said earlier, there might be a case of oversaturation in the vectors and therefore a loss of information on the complex intricacies in the data since binary vectors were used to encode the data. Interesting avenues might include using real-valued vectors to generate neighborhood-encodings. This algorithm could then be coupled with weighted additions to avoid oversaturation of vectors. Instead of relying solely on random amino acid vectors for neighborhood-encoding the residues, future research could investigate the potential utility of alternative amino acid representations, such as the projected ESM-2 embeddings, either real-valued or binary.

Lastly, the size of the training dataset could also be a contributing factor. Given the computational constraints of this study, we were limited in the amount of data we could use for training. However, machine learning models, especially deep neural networks, often benefit from larger datasets. Increasing the size of the training dataset could provide our models with more examples to learn from, potentially improving their performance.

In order to benchmark our study against the capabilities of state-of-the-art protein language models, we collected the available results of other pro-

tein language models on similar experiments. The models include ESM-1b [44], NetSurfP 2.0 [80], its successor NetSurfP 3.0 [84] and ProtTrans' best-performing model; ProtT5-XL-U50 [51]. ESM-1b is a model by Meta AI, trained on a large corpus of approximately 86 billion amino acid residues. It consists of around 670 million parameters and utilizes a transformer architecture together with evolutionary data. NetsurfP 2.0 and its successor NetSurf 3.0 are models comprising convolutional neural network (CNN) and bidirectional long short-term (biLSTM) layers. Despite not relying on a transformer-based architecture and having been trained on a comparatively smaller dataset, they exhibit state-of-the-art performance. The distinction between these two methods lies in their input configurations. ProtT5-XL-U50 is a large transformer-based model comprising 3 billion parameters, trained on UniRef50 which comprises roughly 45 million sequences [85].

When compared to the performance of state-of-the-art protein language models in Table 5.4, our models fall short in performance. This underscores the complexity of protein secondary structure prediction and the need for models that can effectively learn from the intricate patterns in the data.

6. CONCLUSION AND FUTURE PERSPECTIVES

This thesis has investigated the potential applications of hyperdimensional computing in the field of bioinformatics, specifically protein sequence research. Starting from an overview of protein research, we identified the need for more efficient computational methods. Responding to this need, we explored the principles of hyperdimensional computing and developed encoding strategies for amino acids and protein sequences. We tested these strategies on the PhaLP protein sequence database and used the resulting embeddings in prediction tasks. Our findings indicate potential benefits of these methods, despite some challenges, and provide a foundation for further research in this area.

First in Chapter 1, we discussed the history and advancements in molecular biology and bioinformatics made in the mid-20th 21st century that revolutionized our understanding of the genetic code, sequence analyses and protein structures. In particular, the integration of natural language processing (NLP) techniques into protein research that has further expanded the horizons of bioinformatics.

In response to the need for more efficient algorithms and learning methods in the realm of protein language modeling, we presented hyperdimensional computing, a concept inspired by the human brain's capacity to learn, adapt and recognize semantic relationships. The power of this computing framework was demonstrated by illustrating its operations and applying it to several datasets.

In our exploration of the potential applications of hyperdimensional computing in protein research, we have set a workflow in Chapter 3. This process involved encoding amino acids and protein sequences into hyperdimensional embeddings, subsequently leveraging these embeddings in prediction tasks. Our initial focus centered on identifying appropriate encoding mechanisms for both amino acids and proteins. Multiple strategies for each

were illustrated and evaluated using visual projections. Notably, we observed that existing amino acid embeddings, such as those from the ESM-2 model, proved to be useful as starting points for amino acid encodings. Moreover, we ventured into exploring alternative methods that could potentially enhance our study.

We then applied these amino acid- and protein-encoding methods to encode sequences of the PhaLP database in Chapter 4. On top of this, we explored a multitude of methods to learn and predict classes of these sequences using the generated embeddings. We found a hyperdimensional computing-based method, OnlineHD, to be particularly performing well on classification tasks on our sequence embeddings, achieving competitive performance levels compared to other established machine learning methodologies in some cases. This substantiated the effectiveness of our sequence encoding methods, as the models were able to accurately learn and predict from these embeddings.

In Chapter 5, we focused on our exploration of perceptron-based models for context-aware protein residue learning, utilizing neighborhood-encoded hyperdimensional vectors as an input. Our motivation for this endeavor was to explore for potential avenues to design computationally efficient alternatives to transformer-based models, which, despite their state-of-the-art performance, impose significant computational demands. Our methodology involved training different perceptron-based architectures (specifically, single-layer perceptron and multi-layer perceptron models) on NetsurfP 2.0's training dataset. The experiments with these models led to poor results, revealing insights into the performance of perceptron models with high-dimensional inputs. This exploration, while not leading to a model that outperforms existing state-of-the-art models, has provided insights into the challenges of designing efficient models for context-aware protein residue learning within the framework of hyperdimensional computing.

As we navigated through these processes, the issue of vectors potentially becoming oversaturated surfaced depending on the method used. We saw that prediction methods such as OnlineHD and XGBoost classifiers capture the information in hyperdimensional sequence embeddings very well, but that naively bundled vectors of sequences or neighborhood-encoded amino acid vectors lost most of the input information, which highlights the need for further research in this area.

As for future perspectives, there are many possibilities that could be taken on from here. If saturation of bundling vectors arises as a problem, algorithms could be developed to mitigate this problem. An innovative approach would be to consider the development of end-to-end methods, where the dimensionality and the maximum bundling capacity are integrated as hyperparameters. This could enhance both the flexibility and performance of the system.

Another promising avenue lies in the fusion of successful concepts from state-of-the-art methods, such as self-supervision, pretraining, and self-attention, with principles inherent to hyperdimensional computing. This synergy might result in a new generation of effective protein language modeling tools.

In expanding upon the fundamental operations of hyperdimensional computing, one could focus on the creation of more interpretable models. Given the inherently reversible nature of bundling and binding operations in hyperdimensional computing, one approach could involve leveraging these unique properties to construct highly interpretable networks using HDVs. This could offer a significant advantage over current models which are often referred to as "black boxes" due to their lack of interpretability.

Further exploration in this area could help to unlock the full potential of hyperdimensional computing in bioinformatics and could provide valuable insights for other fields where high-dimensional data and complex patterns are prevalent.

BIBLIOGRAPHY

[1] Criel, B., Taelman, S. *et al.* (2021). PhaLP: A Database for the Study of Phage Lytic Proteins and Their Evolution. *Viruses*, 13(7):1240. Publisher: MDPI, AG.

[2] Watson, J.D. and Crick, F.H.C. (1953). Molecular Structure of Nucleic Acids: A Structure for Deoxyribose Nucleic Acid. *Nature*, 171(4356):737–738. Publisher: Springer Science and Business Media LLC.

[3] Cobb, M. and Comfort, N. (2023). What Rosalind Franklin truly contributed to the discovery of DNA's structure. *Nature*, 616(7958):657–660. Publisher: Springer Science and Business Media LLC.

[4] Crick, F. (1970). Central Dogma of Molecular Biology. *Nature*, 227(5258):561–563. Publisher: Springer Science and Business Media LLC.

[5] Sanger, F. and Thompson, E.O.P. (1953). The amino-acid sequence in the glycyl chain of insulin. 1. The identification of lower peptides from partial hydrolysates. *Biochemical Journal*, 53(3):353–366. Publisher: Portland Press Ltd.

[6] Dayhoff, M.O. and Ledley, R.S. (1962). Comprotein. In *Proceedings of the December 4-6, 1962, fall joint computer conference on - AFIPS '62 (Fall)*. ACM Press.

[7] Hersh, R.T., Eck, R.V. *et al.* (1967). Atlas of Protein Sequence and Structure, 1966. *Systematic Zoology*, 16(3):262. Publisher: Oxford University Press (OUP).

[8] Koonin, E.V. and Novozhilov, A.S. (2009). Origin and evolution of the genetic code: The universal enigma. *IUBMB Life*, 61(2):99–111. Publisher: Wiley.

[9] Needleman, S.B. and Wunsch, C.D. (1970). A general method applicable to the search for similarities in the amino acid sequence of two proteins. *Journal of Molecular Biology*, 48(3):443–453. ISSN 0022-2836.

[10] Sanger, F., Air, G.M. *et al.* (1977). Nucleotide sequence of bacteriophage X174 DNA. *Nature*, 265(5596):687–695. Publisher: Springer Science and Business Media LLC.

[11] Smith, T.F. and Waterman, M.S. (1981). Identification of common molecular subsequences. *Journal of Molecular Biology*, 147(1):195–197. ISSN 0022-2836.

[12] Lipman, D.J. and Pearson, W.R. (1985). Rapid and Sensitive Protein Similarity Searches. *Science*, 227(4693):1435–1441. _eprint: https://www.science.org/doi/pdf/10.1126/science.2983426.

[13] Nurk, S., Koren, S. *et al.* (2022). The complete sequence of a human genome. *Science*, 376(6588):44–53. Publisher: American Association for the Advancement of Science (AAAS).

[14] Margulies, M., Egholm, M. *et al.* (2005). Genome sequencing in microfabricated high-density picolitre reactors. *Nature*, 437(7057):376–380. Publisher: Springer Science and Business Media LLC.

[15] AlQuraishi, M. (2019). AlphaFold at CASP13. *Bioinformatics*, 35(22):4862–4865. Publisher: Oxford University Press (OUP).

[16] Kendrew, J.C., Bodo, G. *et al.* (1958). A Three-Dimensional Model of the Myoglobin Molecule Obtained by X-Ray Analysis. *Nature*, 181(4610):662–666. Publisher: Springer Science and Business Media LLC.

[17] Fruton, J.S. (1979). Early Theories of Protein Structure. *Annals of the New York Academy of Sciences*, 325(1):1–20.

[18] Edman, P. and Begg, G. (1967). A Protein Sequenator. *European Journal of Biochemistry*, 1(1):80–91. Publisher: Wiley.

[19] Altschul, S.F., Gish, W. *et al.* (1990). Basic local alignment search tool. *Journal of Molecular Biology*, 215(3):403–410. ISSN 0022-2836.

[20] Murata, M., Richardson, J.S. *et al.* (1985). Simultaneous comparison of three protein sequences. *Proceedings of the National Academy of Sciences*, 82(10):3073–3077. Publisher: Proceedings of the National Academy of Sciences.

[21] Higgins, D.G. and Sharp, P.M. (1988). CLUSTAL: a package for performing multiple sequence alignment on a microcomputer. *Gene*, 73(1):237–244. Publisher: Elsevier BV.

[22] Edgar, R.C. (2004). MUSCLE: multiple sequence alignment with high accuracy and high throughput. *Nucleic Acids Research*, 32(5):1792–1797. Publisher: Oxford University Press (OUP).

[23] (2016). Phylogeny in Multiple Sequence Alignments. In *Multiple Biological Sequence Alignment: Scoring Functions, Algorithms and Applications*, pages 103–112. John Wiley & Sons, Inc.

[24] Jou, W.M., Haegeman, G. *et al.* (1972). Nucleotide Sequence of the Gene Coding for the Bacteriophage MS2 Coat Protein. *Nature*, 237(5350):82–88. Publisher: Springer Science and Business Media LLC.

[25] Benson, D.A., Cavanaugh, M. *et al.* (2012). GenBank. *Nucleic Acids Research*, 41(D1):D36–D42. Publisher: Oxford University Press (OUP).

[26] Cunningham, F., Allen, J.E. *et al.* (2021). Ensembl 2022. *Nucleic Acids Research*, 50(D1):D988–D995. Publisher: Oxford University Press (OUP).

[27] Burgin, J., Ahamed, A. *et al.* (2022). The European Nucleotide Archive in 2022. *Nucleic Acids Research*, 51(D1):D121–D125. Publisher: Oxford University Press (OUP).

[28] (2022). 'New era in digital biology': AI reveals structures of nearly all known proteins.

[29] Levinthal, C. (1968). Are there pathways for protein folding? *Journal de Chimie Physique*, 65:44–45. Publisher: EDP Sciences.

[30] Ptitsyn, O. (1991). How does protein synthesis give rise to the 3D-structure? *FEBS Letters*, 285(2):176–181. _eprint: https://febs.onlinelibrary.wiley.com/doi/pdf/10.1016/0014-5793%2891%2980799-9.

[31] König, S., Obermann, W.M.J. *et al.* (2022). The Current State-of-the-Art Identification of Unknown Proteins Using Mass Spectrometry Exemplified on De Novo Sequencing of a Venom Protease from Bothrops moojeni. *Molecules*, 27(15). ISSN 1420-3049.

[32] Altschul, S. (1997). Gapped BLAST and PSI-BLAST: a new generation of protein database search programs. *Nucleic Acids Research*, 25(17):3389–3402. Publisher: Oxford University Press (OUP).

[33] Steinegger, M., Meier, M. *et al.* (2019). HH-suite3 for fast remote homology detection and deep protein annotation. *BMC Bioinformatics*, 20(1). Publisher: Springer Science and Business Media LLC.

[34] Steinegger, M. and Söding, J. (2017). MMseqs2 enables sensitive protein sequence searching for the analysis of massive data sets. *Nature Biotechnology*, 35(11):1026–1028. Publisher: Springer Science and Business Media LLC.

[35] Berman, H.M. (2000). The Protein Data Bank. *Nucleic Acids Research*, 28(1):235–242. Publisher: Oxford University Press (OUP).

[36] Bateman, a.A., Martin, M.J. *et al.* (2022). UniProt: the Universal Protein Knowledgebase in 2023. *Nucleic Acids Research*, 51(D1):D523–D531. Publisher: Oxford University Press (OUP).

[37] Yip, K.M., Fischer, N. *et al.* (2020). Atomic-resolution protein structure determination by cryo-EM. *Nature*, 587(7832):157–161. Publisher: Springer Science and Business Media LLC.

[38] Porta-Pardo, E., Ruiz-Serra, V. *et al.* (2022). The structural coverage of the human proteome before and after AlphaFold. *PLOS Computational Biology*, 18(1):e1009818. Publisher: Public Library of Science (PLoS).

[39] Leaver-Fay, A., Tyka, M. *et al.* (2011). Rosetta3. In *Computer Methods, Part C*, pages 545–574. Elsevier.

[40] Bepler, T. and Berger, B. (2021). Learning the protein language: Evolution, structure, and function. *Cell Systems*, 12(6):654–669.e3. Publisher: Elsevier BV.

[41] Jumper, J., Evans, R. *et al.* (2021). Highly accurate protein structure prediction with AlphaFold. *Nature*, 596(7873):583–589. Publisher: Springer Science and Business Media LLC.

[42] Callaway, E. (2022). After AlphaFold: protein-folding contest seeks next big breakthrough. *Nature*, 613(7942):13–14. Publisher: Springer Science and Business Media LLC.

[43] Ofer, D., Brandes, N. *et al.* (2021). The language of proteins: NLP, machine learning and protein sequences. *Computational and Structural Biotechnology Journal*, 19:1750–1758. Publisher: Elsevier BV.

[44] Rives, A., Meier, J. *et al.* (2019). Biological structure and function emerge from scaling unsupervised learning to 250 million protein sequences. Publisher: Cold Spring Harbor Laboratory.

[45] Peters, M.E., Neumann, M. *et al.* (2018). Deep contextualized word representations.

[46] Devlin, J., Chang, M.W. *et al.* (2018). BERT: Pre-training of Deep Bidirectional Transformers for Language Understanding.

[47] Brown, T.B., Mann, B. *et al.* (2020). Language Models are Few-Shot Learners.

[48] OpenAI (2023). GPT-4 Technical Report.

[49] Vaswani, A., Shazeer, N. *et al.* (2017). Attention Is All You Need.

[50] Rao, R., Bhattacharya, N. *et al.* (2019). Evaluating Protein Transfer Learning with TAPE.

[51] Elnaggar, A., Heinzinger, M. *et al.* (2020). ProtTrans: Towards Cracking the Language of Life's Code Through Self-Supervised Deep Learning and High Performance Computing.

[52] Lin, Z., Akin, H. *et al.* (2022). Evolutionary-scale prediction of atomic level protein structure with a language model. Publisher: Cold Spring Harbor Laboratory.

[53] Narayanan, D., Shoeybi, M. *et al.* (2021). Efficient Large-Scale Language Model Training on GPU Clusters Using Megatron-LM.

[54] Luccioni, A.S., Viguier, S. *et al.* (2022). Estimating the Carbon Footprint of BLOOM, a 176B Parameter Language Model.

[55] World Resources Institute, Greenhouse Gas (GHG) Emissions Climate Watch, climatewatchdata.org/ghg-emissions.

[56] Kanerva, P. (2009). Hyperdimensional Computing: An Introduction to Computing in Distributed Representation with High-Dimensional Random Vectors. *Cognitive Computation*, 1(2):139–159. ISSN 1866-9956.

[57] Plate, T. (1995). Holographic reduced representations. *IEEE Transactions on Neural Networks*, 6(3):623–641.

[58] Kanerva, P. (1994). The Spatter Code for Encoding Concepts at Many Levels. *ICANN '94*, pages 226–229. ISBN: 978-1-4471-2097-1 Place: London Publisher: Springer London.

[59] Thomas, A., Dasgupta, S. *et al.* (2021). A Theoretical Perspective on Hyperdimensional Computing. *Journal of Artificial Intelligence Research*, 72:215–249. Publisher: AI Access Foundation.

[60] Bezanson, J., Edelman, A. *et al.* (2017). Julia: A fresh approach to numerical computing. *SIAM Review*, 59(1):65–98. Publisher: SIAM.

[61] Schmuck, M., Benini, L. *et al.* (2019). Hardware Optimizations of Dense Binary Hyperdimensional Computing: Rematerialization of Hypervectors, Binarized Bundling, and Combinational Associative Memory. *J. Emerg. Technol. Comput. Syst.*, 15(4). ISSN 1550-4832. Place: New York, NY, USA Publisher: Association for Computing Machinery.

[62] Ge, L. and Parhi, K.K. (2020). Classification Using Hyperdimensional Computing: A Review. *IEEE Circuits and Systems Magazine*, 20(2):30–47. Publisher: Institute of Electrical and Electronics Engineers (IEEE).

[63] Learning, U.M. (2016). Zoo Animal Classification. Publication Title: Kaggle.

[64] Grisoni, F., Neuhaus, C.S. *et al.* (2019). 'De novo design of anticancer peptides by ensemble artificial neural networks. *Journal of Molecular Modeling*, 25(5):122. ISSN 0948-5023.

[65] Zou, Z., Chen, H. *et al.* (2022). BioHD. In *Proceedings of the 49th Annual International Symposium on Computer Architecture*. ACM.

[66] Sneath, P.H.A. (1966). Relations between chemical structure and biological activity in peptides. *Journal of Theoretical Biology*, 12(2):157–195. Publisher: Elsevier BV.

[67] Mitchell, M. (1998). *An Introduction to Genetic Algorithms*. The MIT Press.

[68] Wilde, A., Thiem, D. *et al.* (2021). Evolutionary.jl.

[69] Henikoff, S. and Henikoff, J.G. (1992). Amino acid substitution matrices from protein blocks. *Proceedings of the National Academy of Sciences*, 89(22):10915–10919. Publisher: Proceedings of the National Academy of Sciences.

[70] Grantham, R. (1974). Amino Acid Difference Formula to Help Explain Protein Evolution. *Science*, 185(4154):862–864. Publisher: American Association for the Advancement of Science (AAAS).

[71] Yu, T., Zhang, Y. *et al.* (2022). Understanding Hyperdimensional Computing for Parallel Single-Pass Learning.

[72] Rodríguez-Rubio, L., Gutiérrez, D. *et al.* (2015). Phage lytic proteins: biotechnological applications beyond clinical antimicrobials. *Critical Reviews in Biotechnology*, pages 1–11. Publisher: Informa UK Limited.

[73] Darby, E.M., Trampari, E. *et al.* (2022). Molecular mechanisms of antibiotic resistance revisited. *Nature Reviews Microbiology*, 21(5):280–295. Publisher: Springer Science and Business Media LLC.

[74] Heinzinger, M., Elnaggar, A. *et al.* (2019). Modeling aspects of the language of life through transfer-learning protein sequences. *BMC Bioinformatics*, 20(1). Publisher: Springer Science and Business Media LLC.

[75] Breiman, L. (2001). Random forests. *Machine Learning*, 45(1):5–32. Publisher: Springer Science and Business Media LLC.

[76] Hernández-Cane, A., Matsumoto, N. *et al.* (2021). OnlineHD: Robust, Efficient, and Single-Pass Online Learning Using Hyperdimensional System. *2021 Design, Automation & Test in Europe Conference & Exhibition (DATE)*, pages 56–61.

[77] Chen, T. and Guestrin, C. (2016). XGBoost: A Scalable Tree Boosting System. *CoRR*, abs/1603.02754.

[78] Rosenblatt, F. (1958). The perceptron: A probabilistic model for information storage and organization in the brain. *Psychological Review*, 65(6):386–408. Publisher: American Psychological Association (APA).

[79] Schmidhuber, J. (2022). Annotated History of Modern AI and Deep Learning.

[80] Klausen, M.S., Jespersen, M.C. *et al.* (2019). NetSurfP-2.0: Improved prediction of protein structural features by integrated deep learning. *Proteins: Structure, Function, and Bioinformatics*, 87(6):520–527. Publisher: Wiley.

[81] Kabsch, W. and Sander, C. (1983). Dictionary of protein secondary structure: Pattern recognition of hydrogen-bonded and geometrical features. *Biopolymers*, 22(12):2577–2637. Publisher: Wiley.

[82] Yang, Y., Gao, J. *et al.* (2016). Sixty-five years of the long march in protein secondary structure prediction: the final stretch? *Briefings in Bioinformatics*, page bbw129. Publisher: Oxford University Press (OUP).

[83] Moult, J., Fidelis, K. *et al.* (2017). Critical assessment of methods of protein structure prediction (CASP)-Round XII. *Proteins: Structure, Function, and Bioinformatics*, 86:7–15. Publisher: Wiley.

[84] Høie, M.H., Kiehl, E.N. *et al.* (2022). NetSurfP-3.0: accurate and fast prediction of protein structural features by protein language models and deep learning. *Nucleic Acids Research*, 50(W1):W510–W515. Publisher: Oxford University Press (OUP).

[85] Suzek, B.E., Huang, H. *et al.* (2007). UniRef: comprehensive and non-redundant UniProt reference clusters. *Bioinformatics*, 23(10):1282–1288. Publisher: Oxford University Press (OUP).

APPENDIX A

ADDITIONAL INFORMATION ON CHAPTER 3

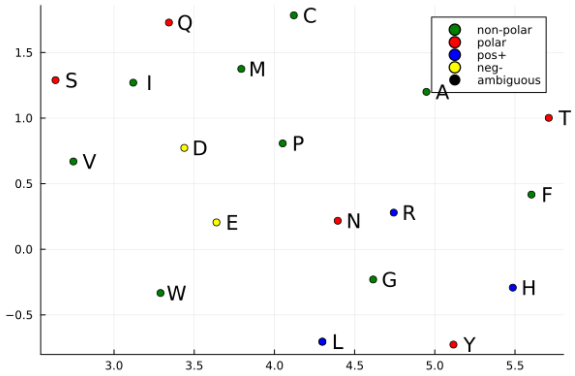

(a) Made starting from random hyperdimensional vectors for each amino acid, $k = 4$.

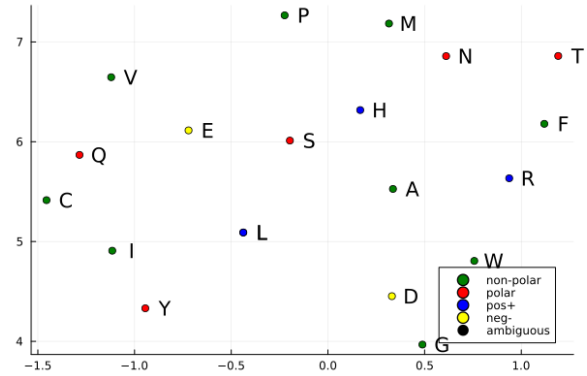

(b) Made starting from random hyperdimensional vectors for each amino acid, $k = 50$.

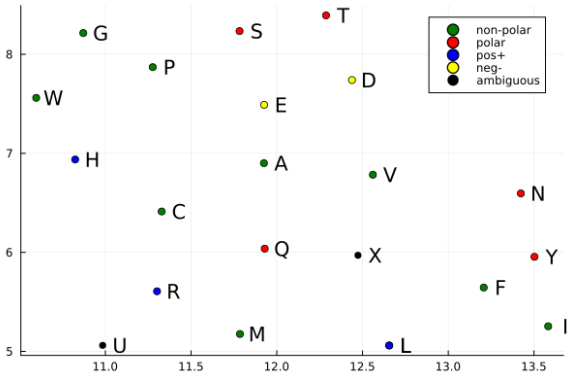

(c) Made starting from extended ESM-2 embeddings for each amino acid, $k = 4$.

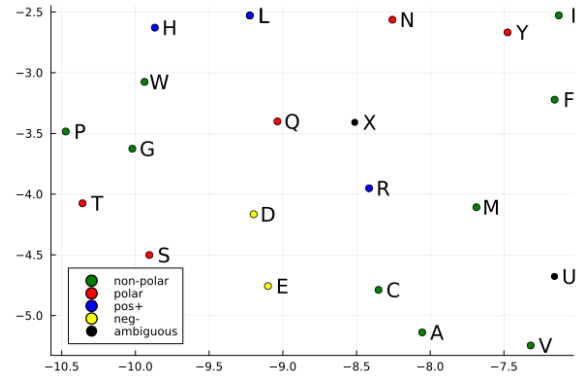

(d) Made starting from extended ESM-2 embeddings for each amino acid, $k = 50$.

Figure A.1: Scatter plot of a two-dimensional UMAP projection of the average amino acid HDVs with neighborhood-information of k encoded. Learned from the human reference proteome. The amino acids are annotated and colored based on their chemical property of polarity.

Table A.1: Target similarities made from Grantham's distance matrix

0.0	0.73	0.87	0.8	0.87	0.73	0.87	0.8	0.8	0.8	0.8	0.87	0.8	0.8	0.8	0.67	0.73	0.73	0.93	0.87
0.73	0.0	0.93	1.0	0.87	0.93	0.93	0.8	0.93	0.8	0.8	0.93	0.93	0.93	0.93	0.8	0.8	0.8	0.87	0.87
0.87	0.93	0.0	0.6	0.93	0.8	0.8	0.93	0.8	1.0	0.93	0.67	0.8	0.73	0.87	0.73	0.8	0.93	1.0	0.93
0.8	1.0	0.6	0.0	0.93	0.87	0.73	0.93	0.67	0.93	0.87	0.73	0.8	0.6	0.73	0.73	0.8	0.87	0.93	0.87
0.87	0.87	0.93	0.93	0.0	0.93	0.8	0.73	0.93	0.73	0.73	0.93	1.0	0.93	0.93	0.87	0.87	0.8	0.67	0.53
0.73	0.93	0.8	0.87	0.93	0.0	0.87	1.0	0.87	1.0	0.93	0.73	0.87	0.87	0.87	0.73	0.87	0.93	0.87	0.93
0.87	0.93	0.8	0.73	0.8	0.87	0.0	0.93	0.8	0.93	0.87	0.67	0.87	0.73	0.73	0.8	0.87	0.93	0.87	0.6
0.8	0.8	0.93	0.93	0.73	1.0	0.93	0.0	0.93	0.6	0.67	0.93	0.93	0.93	0.93	0.87	0.8	0.53	0.93	0.8
0.8	0.93	0.8	0.67	0.93	0.87	0.8	0.93	0.0	0.87	0.8	0.73	0.8	0.67	0.6	0.73	0.8	0.87	0.93	0.87
0.8	0.8	1.0	0.93	0.73	1.0	0.93	0.6	0.87	0.0	0.6	0.93	0.93	0.87	0.87	0.87	0.8	0.67	0.87	0.8
0.8	0.8	0.93	0.87	0.73	0.93	0.87	0.67	0.8	0.6	0.0	0.87	0.87	0.73	0.8	0.8	0.8	0.67	0.8	0.8
0.87	0.93	0.67	0.73	0.93	0.73	0.67	0.93	0.73	0.93	0.87	0.0	0.87	0.73	0.73	0.67	0.73	0.93	1.0	0.87
0.8	0.93	0.8	0.8	1.0	0.87	0.87	0.93	0.8	0.93	0.87	0.87	0.0	0.8	0.87	0.8	0.8	0.87	1.0	0.93
0.8	0.93	0.73	0.6	0.93	0.87	0.73	0.93	0.67	0.87	0.73	0.73	0.8	0.0	0.67	0.73	0.8	0.87	0.87	0.8
0.8	0.93	0.87	0.73	0.93	0.87	0.73	0.93	0.6	0.87	0.8	0.73	0.87	0.67	0.0	0.8	0.8	0.93	0.93	0.87
0.67	0.8	0.73	0.73	0.87	0.73	0.8	0.87	0.73	0.87	0.8	0.67	0.8	0.73	0.8	0.0	0.67	0.87	0.93	0.87
0.73	0.8	0.8	0.8	0.87	0.87	0.87	0.8	0.8	0.8	0.8	0.73	0.8	0.8	0.8	0.67	0.0	0.73	0.87	0.87
0.73	0.8	0.93	0.87	0.8	0.93	0.93	0.53	0.87	0.67	0.67	0.93	0.87	0.87	0.93	0.87	0.73	0.0	0.93	0.8
0.93	0.87	1.0	0.93	0.67	0.87	0.87	0.93	0.93	0.87	0.8	1.0	1.0	0.87	0.93	0.93	0.87	0.93	0.0	0.6
0.87	0.87	0.93	0.87	0.53	0.93	0.6	0.8	0.87	0.8	0.8	0.87	0.93	0.8	0.87	0.87	0.87	0.8	0.6	0.0

Table A.2: Achieved similarities targeting Grantham's distance matrix

0.0	0.49	0.49	0.48	0.48	0.49	0.5	0.49	0.49	0.5	0.49	0.49	0.49	0.49	0.49	0.48	0.5	0.51	0.49	0.49
0.49	0.0	0.49	0.5	0.49	0.49	0.49	0.5	0.5	0.48	0.5	0.5	0.5	0.49	0.48	0.49	0.49	0.49	0.49	0.49
0.49	0.49	0.0	0.49	0.49	0.49	0.49	0.49	0.49	0.5	0.49	0.49	0.5	0.49	0.49	0.5	0.49	0.5	0.49	0.49
0.48	0.5	0.49	0.0	0.49	0.48	0.5	0.5	0.49	0.49	0.49	0.5	0.5	0.5	0.49	0.5	0.49	0.49	0.49	0.49
0.48	0.49	0.49	0.49	0.0	0.5	0.5	0.5	0.49	0.49	0.5	0.5	0.5	0.49	0.5	0.5	0.51	0.51	0.5	0.49
0.49	0.49	0.49	0.48	0.5	0.0	0.5	0.49	0.5	0.49	0.49	0.5	0.49	0.49	0.49	0.5	0.5	0.49	0.5	0.5
0.5	0.49	0.49	0.5	0.5	0.5	0.0	0.5	0.51	0.5	0.5	0.5	0.5	0.49	0.49	0.49	0.49	0.5	0.48	0.49
0.49	0.5	0.49	0.5	0.5	0.49	0.5	0.0	0.48	0.49	0.49	0.51	0.5	0.5	0.49	0.5	0.49	0.5	0.5	0.5
0.49	0.5	0.49	0.49	0.49	0.5	0.51	0.48	0.0	0.5	0.49	0.5	0.5	0.49	0.5	0.5	0.48	0.49	0.49	0.49
0.5	0.48	0.5	0.49	0.49	0.49	0.5	0.49	0.5	0.0	0.5	0.5	0.49	0.49	0.49	0.49	0.49	0.5	0.5	0.48
0.49	0.5	0.49	0.49	0.5	0.49	0.5	0.49	0.49	0.5	0.0	0.49	0.49	0.51	0.5	0.49	0.5	0.5	0.49	0.49
0.49	0.5	0.49	0.5	0.5	0.5	0.5	0.51	0.5	0.5	0.49	0.0	0.5	0.49	0.5	0.49	0.5	0.49	0.5	0.49
0.49	0.5	0.5	0.5	0.5	0.49	0.5	0.5	0.5	0.49	0.49	0.5	0.0	0.49	0.5	0.49	0.5	0.49	0.5	0.48
0.49	0.49	0.49	0.5	0.49	0.49	0.49	0.5	0.49	0.49	0.51	0.49	0.49	0.0	0.49	0.5	0.5	0.5	0.49	0.5
0.49	0.48	0.49	0.49	0.5	0.49	0.49	0.49	0.5	0.49	0.5	0.5	0.5	0.49	0.0	0.49	0.49	0.49	0.5	0.5
0.48	0.49	0.5	0.5	0.5	0.5	0.49	0.5	0.5	0.49	0.49	0.49	0.49	0.5	0.49	0.0	0.49	0.5	0.49	0.5
0.5	0.49	0.49	0.49	0.51	0.5	0.49	0.49	0.48	0.49	0.5	0.5	0.5	0.5	0.49	0.49	0.0	0.5	0.5	0.5
0.51	0.49	0.5	0.49	0.51	0.49	0.5	0.5	0.49	0.5	0.5	0.49	0.49	0.5	0.49	0.5	0.5	0.0	0.49	0.48
0.49	0.49	0.49	0.49	0.5	0.5	0.48	0.5	0.49	0.5	0.49	0.5	0.5	0.49	0.5	0.49	0.5	0.49	0.0	0.5
0.49	0.49	0.49	0.49	0.49	0.5	0.49	0.5	0.49	0.48	0.49	0.49	0.48	0.5	0.5	0.5	0.5	0.48	0.5	0.0

Table A.3: Target similarities made from BLOSUM62 matrix

0.0	0.73	0.87	0.8	0.87	0.73	0.87	0.8	0.8	0.8	0.8	0.87	0.8	0.8	0.8	0.67	0.73	0.73	0.93	0.87
0.73	0.0	0.93	1.0	0.87	0.93	0.93	0.8	0.93	0.8	0.8	0.93	0.93	0.93	0.93	0.8	0.8	0.8	0.87	0.87
0.87	0.93	0.0	0.6	0.93	0.8	0.8	0.93	0.8	1.0	0.93	0.67	0.8	0.73	0.87	0.73	0.8	0.93	1.0	0.93
0.8	1.0	0.6	0.0	0.93	0.87	0.73	0.93	0.67	0.93	0.87	0.73	0.8	0.6	0.73	0.73	0.8	0.87	0.93	0.87
0.87	0.87	0.93	0.93	0.0	0.93	0.8	0.73	0.93	0.73	0.73	0.93	1.0	0.93	0.93	0.87	0.87	0.8	0.67	0.53
0.73	0.93	0.8	0.87	0.93	0.0	0.87	1.0	0.87	1.0	0.93	0.73	0.87	0.87	0.87	0.73	0.87	0.93	0.87	0.93
0.87	0.93	0.8	0.73	0.8	0.87	0.0	0.93	0.8	0.93	0.87	0.67	0.87	0.73	0.73	0.8	0.87	0.93	0.87	0.6
0.8	0.8	0.93	0.93	0.73	1.0	0.93	0.0	0.93	0.6	0.67	0.93	0.93	0.93	0.93	0.87	0.8	0.53	0.93	0.8
0.8	0.93	0.8	0.67	0.93	0.87	0.8	0.93	0.0	0.87	0.8	0.73	0.8	0.67	0.6	0.73	0.8	0.87	0.93	0.87
0.8	0.8	1.0	0.93	0.73	1.0	0.93	0.6	0.87	0.0	0.6	0.93	0.93	0.87	0.87	0.87	0.8	0.67	0.87	0.8
0.8	0.8	0.93	0.87	0.73	0.93	0.87	0.67	0.8	0.6	0.0	0.87	0.87	0.73	0.8	0.8	0.8	0.67	0.8	0.8
0.87	0.93	0.67	0.73	0.93	0.73	0.67	0.93	0.73	0.93	0.87	0.0	0.87	0.73	0.73	0.67	0.73	0.93	1.0	0.87
0.8	0.93	0.8	0.8	1.0	0.87	0.87	0.93	0.8	0.93	0.87	0.87	0.0	0.8	0.87	0.8	0.8	0.87	1.0	0.93
0.8	0.93	0.73	0.6	0.93	0.87	0.73	0.93	0.67	0.87	0.73	0.73	0.8	0.0	0.67	0.73	0.8	0.87	0.87	0.8
0.8	0.93	0.87	0.73	0.93	0.87	0.73	0.93	0.6	0.87	0.8	0.73	0.87	0.67	0.0	0.8	0.8	0.93	0.93	0.87
0.67	0.8	0.73	0.73	0.87	0.73	0.8	0.87	0.73	0.87	0.8	0.67	0.8	0.73	0.8	0.0	0.67	0.87	0.93	0.87
0.73	0.8	0.8	0.8	0.87	0.87	0.87	0.8	0.8	0.8	0.8	0.73	0.8	0.8	0.8	0.67	0.0	0.73	0.87	0.87
0.73	0.8	0.93	0.87	0.8	0.93	0.93	0.53	0.87	0.67	0.67	0.93	0.87	0.87	0.93	0.87	0.73	0.0	0.93	0.8
0.93	0.87	1.0	0.93	0.67	0.87	0.87	0.93	0.93	0.87	0.8	1.0	1.0	0.87	0.93	0.93	0.87	0.93	0.0	0.6
0.87	0.87	0.93	0.87	0.53	0.93	0.6	0.8	0.87	0.8	0.8	0.87	0.93	0.8	0.87	0.87	0.87	0.8	0.6	0.0

Table A.4: Achieved similarities targeting BLOSUM62 matrix

0.0	0.49	0.49	0.49	0.5	0.49	0.48	0.49	0.5	0.49	0.5	0.49	0.5	0.5	0.5	0.49	0.49	0.49	0.49	0.49
0.49	0.0	0.5	0.5	0.5	0.49	0.49	0.49	0.49	0.49	0.48	0.49	0.48	0.49	0.49	0.49	0.49	0.49	0.49	0.49
0.49	0.5	0.0	0.49	0.5	0.5	0.5	0.49	0.51	0.48	0.49	0.5	0.49	0.49	0.5	0.5	0.48	0.49	0.49	0.49
0.49	0.5	0.49	0.0	0.49	0.5	0.49	0.5	0.5	0.5	0.5	0.49	0.49	0.51	0.49	0.49	0.49	0.49	0.48	0.49
0.5	0.5	0.5	0.49	0.0	0.5	0.5	0.51	0.5	0.5	0.5	0.5	0.5	0.49	0.5	0.49	0.5	0.49	0.5	0.48
0.49	0.49	0.5	0.5	0.5	0.0	0.49	0.49	0.5	0.5	0.5	0.49	0.49	0.49	0.5	0.49	0.5	0.49	0.49	0.5
0.48	0.49	0.5	0.49	0.5	0.49	0.0	0.5	0.49	0.49	0.5	0.5	0.5	0.5	0.49	0.5	0.49	0.49	0.49	0.49
0.49	0.49	0.49	0.5	0.51	0.49	0.5	0.0	0.5	0.5	0.5	0.5	0.5	0.5	0.5	0.5	0.49	0.49	0.49	0.5
0.5	0.49	0.51	0.5	0.5	0.5	0.49	0.5	0.0	0.49	0.5	0.49	0.49	0.5	0.5	0.49	0.49	0.5	0.49	0.48
0.49	0.49	0.48	0.5	0.5	0.5	0.49	0.5	0.49	0.0	0.5	0.48	0.49	0.49	0.49	0.5	0.49	0.5	0.48	0.49
0.5	0.48	0.49	0.5	0.5	0.5	0.5	0.5	0.5	0.5	0.0	0.5	0.5	0.5	0.5	0.49	0.49	0.49	0.49	0.49
0.49	0.49	0.5	0.49	0.5	0.49	0.5	0.5	0.49	0.48	0.5	0.0	0.51	0.5	0.49	0.49	0.49	0.5	0.49	0.5
0.5	0.48	0.49	0.49	0.5	0.49	0.5	0.5	0.49	0.49	0.5	0.51	0.0	0.5	0.49	0.49	0.49	0.49	0.49	0.49
0.5	0.49	0.49	0.51	0.49	0.49	0.5	0.5	0.5	0.49	0.5	0.5	0.5	0.0	0.5	0.5	0.5	0.49	0.5	0.49
0.5	0.49	0.5	0.49	0.5	0.5	0.49	0.5	0.5	0.49	0.5	0.49	0.49	0.5	0.0	0.5	0.5	0.49	0.49	0.49
0.49	0.49	0.5	0.49	0.49	0.49	0.5	0.5	0.49	0.5	0.49	0.49	0.49	0.5	0.5	0.0	0.49	0.49	0.49	0.49
0.49	0.49	0.48	0.49	0.5	0.5	0.49	0.49	0.49	0.49	0.49	0.49	0.49	0.5	0.5	0.49	0.0	0.49	0.49	0.49
0.49	0.49	0.49	0.49	0.49	0.49	0.49	0.49	0.5	0.5	0.49	0.5	0.49	0.49	0.49	0.49	0.49	0.0	0.49	0.49
0.49	0.49	0.49	0.48	0.5	0.49	0.49	0.49	0.49	0.48	0.49	0.49	0.49	0.5	0.49	0.49	0.49	0.49	0.0	0.49
0.49	0.49	0.49	0.49	0.48	0.5	0.49	0.5	0.48	0.49	0.49	0.5	0.49	0.49	0.49	0.49	0.49	0.49	0.49	0.0

APPENDIX B

ADDITIONAL INFORMATION ON CHAPTER 5

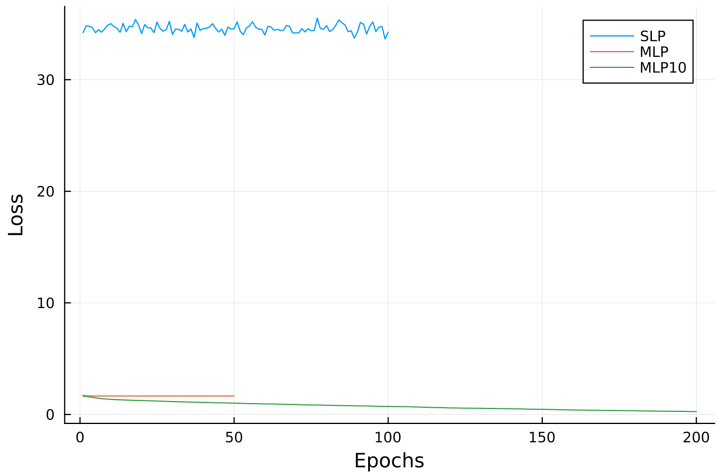

(a) Training losses

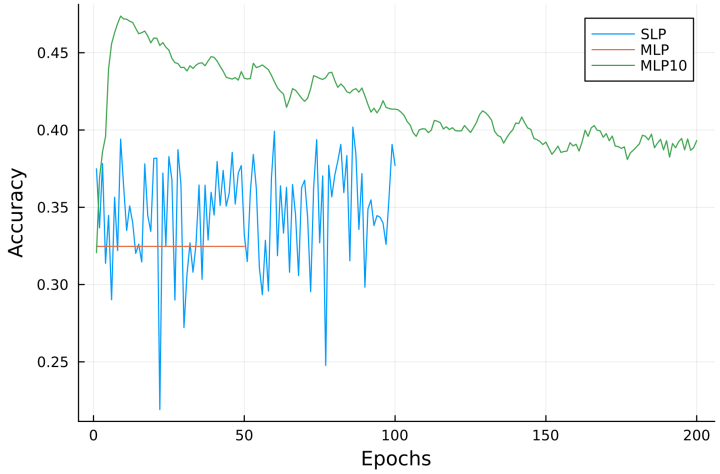

(b) Accuracies

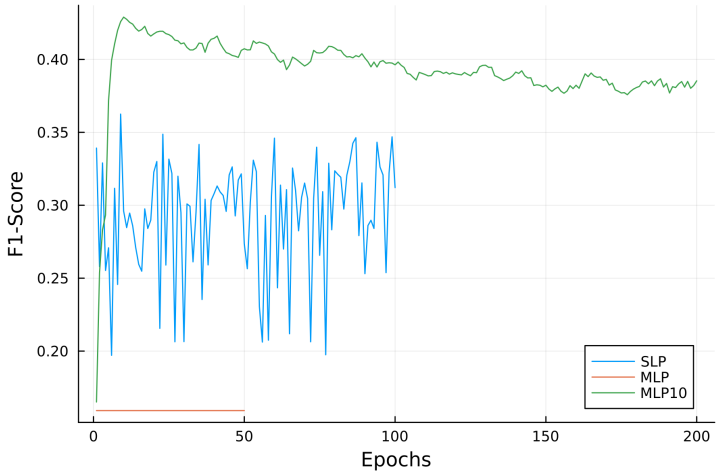

(c) F1-scores

Figure B.1: (a) cross-entropy losses (b) accuracies (c) F1-scores of all perceptron-based configurations tested. Trained with neighborhood-encodings of 60 % of the training dataset of NetSurfP 2.0. Here $n = 25$ and the secondary structure classification is dssp8-based. Note that the SLP and 1-layer MLP model was evaluated using fewer epochs than their 10-layer counterpart.

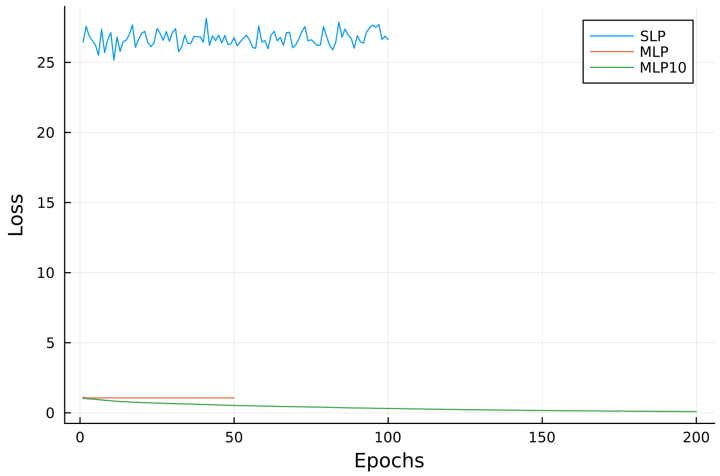

(a) Training losses

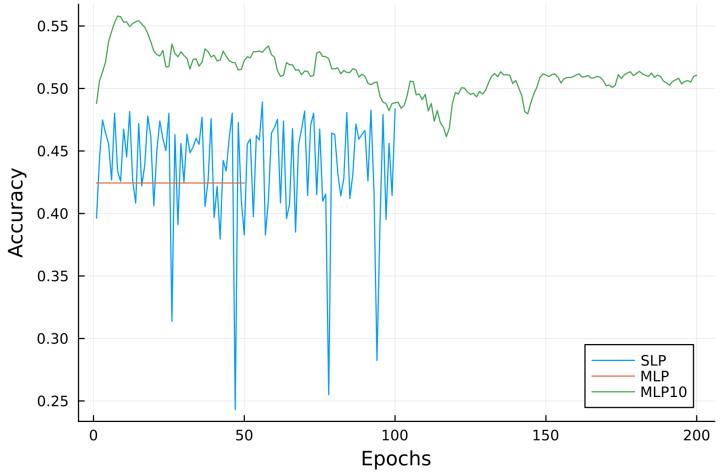

(b) Accuracies

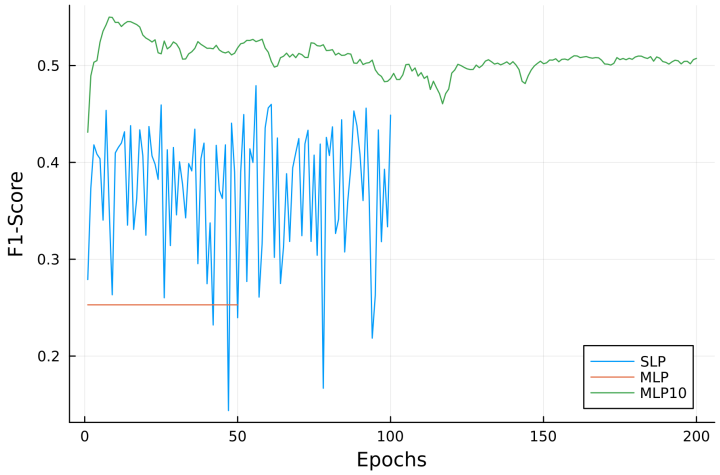

(c) F1-scores

Figure B.2: (a) cross-entropy losses (b) accuracies (c) F1-scores of all perceptron-based configurations tested. Trained with neighborhood-encodings of 60 % of the training dataset of NetSurfP 2.0. Here $n = 100$ and the secondary structure classification is dssp3-based. Note that the SLP and 1-layer MLP model was evaluated using fewer epochs than their 10-layer counterpart.

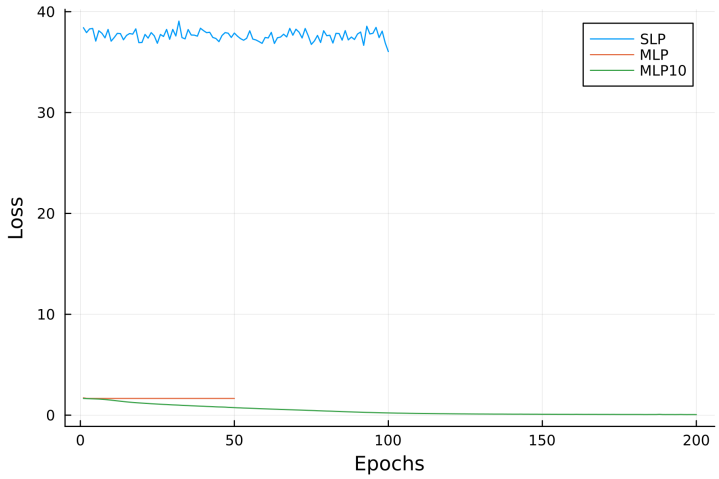

(a) Training losses

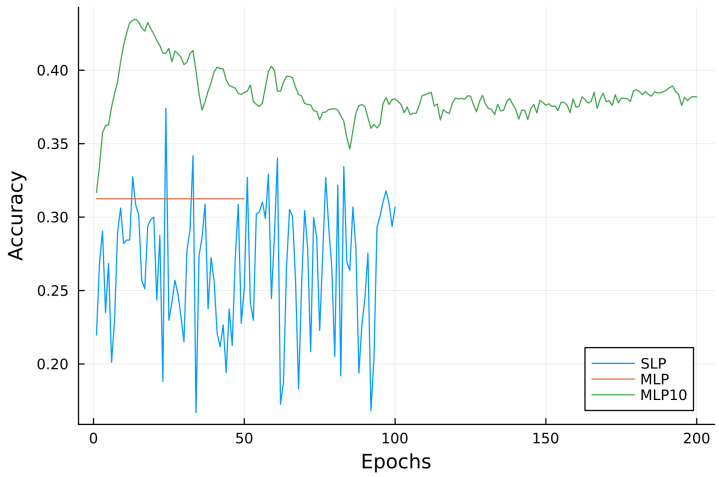

(b) Accuracies

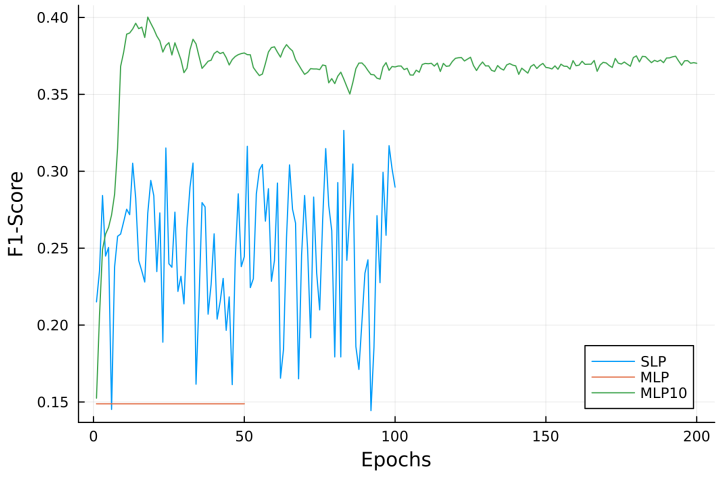

(c) F1-scores

Figure B.3: (a) cross-entropy losses (b) accuracies (c) F1-scores of all perceptron-based configurations tested. Trained with neighborhood-encodings of 60 % of the training dataset of NetSurfP 2.0. Here $n = 100$ and the secondary structure classification is dssp8-based. Note that the SLP and 1-layer MLP model was evaluated using fewer epochs than their 10-layer counterpart.